EXPERIMENTAL STUDY OF RARE-GASES EXCIMER VUV SYSTEM AND H_2 LYMAN-BANDS CALIBRATION

BY

HAOCHEN KE

THESIS

Submitted in partial fulfillment of the requirements
for the degree of Master of Science in Mechanical Engineering
in the Graduate College of the
University of Illinois at Urbana-Champaign, 2012

Urbana, Illinois

Adviser:

Professor Nick G. Glumac

Abstract

An electron impact rare gas excimer vacuum ultra-violet experimental system is custom-designed and tested using an argon and H_2 mixture. An electron flooding system, i.e. filament, is used as the hot electron source. A SiN_x membrane is applied as the entrance foil separating the high vacuum chamber and the test gas chamber. A Custom-designed UV photon intensifier together with high-resolution CCD detector is used to increase the spectrum resolution up to three orders of magnitude higher than previous study. The experimental setting yields sufficiently highly resolved spectrum that could be analyzed in detail. H_2 Lyman-bands are used for the spectrum calibration. A Diatomic code is applied as a simulation reference which is proved to be insufficient for accurate calibration. A Comprehensive calibration using experimental spectrum, diatomic simulation and an H_2 Atlas is performed, and the result shows that the scaling of the spectrometer and detector is off by 0.08 nm, which is a reasonable number for low resolution spectrometer systems.

Acknowledgements

I am very much indebted to Professor Nick Glumac for many helpful remarks and supports during the course of this study. I would also like to show my gratitude to my beloved parents and friends.

Table of Contents

1. Introduction

Dr. Daniel E. Murnick from Rutgers University, New Jersey, published a set of journal papers in the late 1990s reporting his group's work on a new vacuum ultraviolet light source[1, 2]. This light source basically uses a low energy electron beam to excite rare gases such as argon and krypton in order to create an excimer plasma, therefore generating UV light lower than 200nm, which could be used as a deep ultraviolet light source. The plot shown in Figure 1.1 below shows a typical result from the Murnick group[2]. The upper spectrum is the third continuum spectrum of a very pure argon gas excimer, and the lower spectrum is the same spectrum of argon gas slightly contaminated by oxygen. They claimed that the peaks that are easily seen in the lower spectrum are merely the result of oxygen or water vapor impurity. A similar study was conducted by Mills group[16]. They used 12.5 keV low energy electron beam to test rare gas source containing approximately 1% of hydrogen with a monochromator detector. The peaks were again seen in the lower spectrum in Figure 1.2. However, through our study, these peaks don't match the existing lines of neither oxygen, water vapor nor any commonly encountered gas impurities. This contradiction indicates that these lines are not O_2 or H_2O impurity lines, but rather arise from some other species. The even spacing of the lines is peculiar, and although the most likely source is a series of atomic lines, simple identification using common databases has not yielded potential candidates that could explain these features. Furthermore, the spectral resolution of their experimental result is relatively poor, therefore hinders more accurate and detailed spectroscopic analysis. The UIUC combustion diagnostic lab has been doing laser based spectroscopic experiment for decades and has profound experience in both spectroscopic system design and spectrum analysis. Using a high resolution CCD camera and appropriate photon intensifier, spectrum diagnostics studies have been applied to various energy systems and light

sources, such as chemical reacting flow systems and excimer plasma systems. Applying a high resolution Andor CCD camera and a custom designed VUV photon intensifier, we are able to resolve VUV spectra that are up to three orders of magnitude more precise than the spectra resolved by previous studies using a McPherson Model 218 VUV monochromator together with a Hamamatsu R 1080 VUV phototube, which qualifies only for qualitative other than quantitative analysis. Meanwhile, a custom designed testing gas chamber allows us to accurately control the testing gas composition and therefore avoid ambiguous results stemming from the uncertainty of the gas composition. Furthermore, ultrahigh purity level argon and krypton gases have been tested in comparison with the commercial argon for analyzing the role of impurity in the excimer system. Therefore, with the improved experimental design and state-of-the-art diagnostic devices, we attempted to replicate Dr. D. E. Murnick's study, get the spectrum under similar but much more controllable circumstances, study the unspecified spectrum signature of this rare gas plasma source at a much higher resolution level, and try to match this signature to a known chemical species.

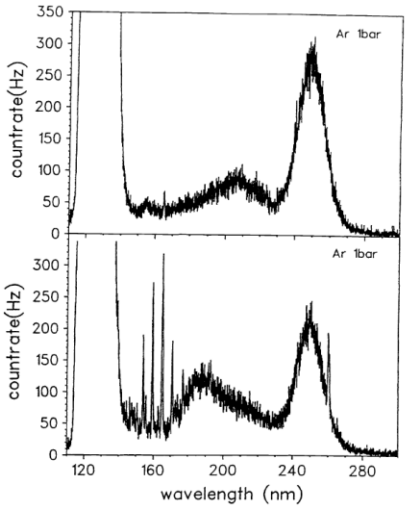

Figure 1.1 Comparison of third continuum Argon of very pure Argon gas and argon gas slightly contaminated by Oxygen[1].

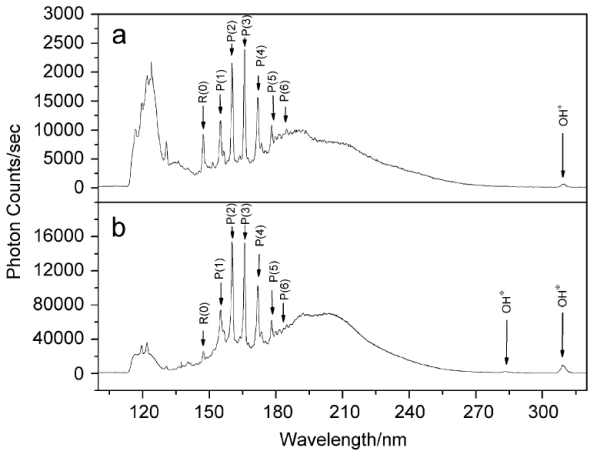

Figure 1.2 (a) and (b). The 100–350 nm spectra of 700–800 Torr, 12.5 keV-electron-beam- maintained plasmas of argon containing about 1% hydrogen by Mills group[16].

2. Literature Review and Background Study

2.1 Excimer VUV Emission Study and Electron Impact Study

In all fields of excimer physics, development of incoherent excimer light sources and excimer lasers, special conditions for excitation of the excimer forming gases is required. On one hand one needs high excitation energy for producing precursor atoms in electronically excited states, and on the other hand the overall gas temperature should be low to allow effective molecule formation[2].

There are various methods for achieving such a situation each with its own advantages and disadvantages[2]. By using pulsed discharges in dense gases, one can achieve atomic excitation when appropriate electric field is applied. The electrons will be accelerated in the discharge to excite the gas atoms through electronic collision. Excimer formation occurs predominantly in the afterglow when the gas cools down allowing molecules to form[2]. This technique is frequently used in excimer lasers. For a homogeneous excitation of dense gas it is, however, often necessary to prevent the discharge from arcing by some pre-ionization using ultraviolet light or ionizing radiation. Another problem with discharges can be erosion of the electrodes which leads to contamination of the gas and optical windows in the system[2].

This contamination problem is avoided by using electrodeless discharges or surface barrier discharges in which the excimer forming gas is not in direct contact with metal electrodes[2].Gellert et al. used dielectric barrier discharge to excite excimer species such as rare-gas dimers and halogen excimers[43]. Boichenko et al. studied radiation characteristics of a cylindrical excilamp at wavelengths of 222nm and 308nm[44]. Vizir' et al. found that a

longitudinal discharge could generate several times higher radiation power than a barrier discharge[45]. Fully continuous excimer formation can be achieved in a certain pressure and current regime of a regular glow discharge of typically 10mbar[46]. Another way of continuous excimer formation is by using a direct current discharge in a dense gas together with a supersonic expansion through a nozzle[47, 48].

Another approach in excimer physics is photoexcitation of the gas atoms into states in which they act as precursors for excimer molecule formation[2]. This method has been successfully used for the assignment of excimer continua to the corresponding molecular transitions for xenon, krypton and argon[49]. Molecular potential curves, transitions and excited state constants can be studied in detail by specifically exciting certain vibrational levels[50]. Electromagnetic radiation was also used as a first step of excimer formation by sending x-rays into a dense gas[51]. Short excitation pulses can be used for kinetic studies. Both synchrotron radiation sources and laser systems are used as tunable light sources. Despite its excellent performance in basic studies this method is not practical for applications where a high output power is needed since accelerators and laser systems are rather sophisticated or bulky devices and inefficient with respect to power conversion[2].

Excitation of gas targets by beams of ionizing particles such as electrons or ions is routinely used for excimer formation. The elements must have an energy high enough to penetrate entrance foil which is strong enough to withstand the pressure differential between the high vacuum chamber in which the particle beam is formed and the gas chamber in which the excimer forms. The elements should loose only a small fraction of their kinetic energy in the entrance foil[2]. Pulsed electron beam excitation using high particle energy (MeV) and high power provided by Marx generator driven accelerators is routinely used for pumping of high power excimer laser

systems[52, 53]. Murnick et al. used silicon nitride membrane as the entrance foil and significantly reduced the acceleration power required for electrons to penetrate the entrance foil without a significant energy loss[1, 2]. Heavy ion beams have also been used in excimer research[54-57].

Recently, the rare gas excimer systems have been extensively studied by various research groups, and the application seems promising. Sankara et al.[90-92] verified the strong continuum peaked at 128nm of argon excimer emission using microhollow cathode discharges (MHCDs). Kubodera et al.[93] reported two new VUV continua centered at 145nm and 163nm by exciting the argon/krypton mixture and krypton/xenon mixture. Masoud et al.[94] studied pure argon and argon/nitrogen and argon/air mixture excimer using cylindrical dielectric barrier discharges (C-DBD). The molecular continuum of xenon centered at 172nm was also studied by various groups[95-100], and the experimental spectrum was also compared with computer modeling by Carman and Mildren[101]. Kurunczi et al.[102] studied high pressure neon with small admixture of hydrogen using microhollow cathode discharge method and observed intense atomic hydrogen Lyman-α and Lyman-β lines. Mühlberger et al.[103] applied argon excimer VUV source together with Single-Photon ionization quadrupole mass spectroscopy to monitor a trace compound. Xenon-excimer radiation was applied by Openländer group[104] to study organic micropollutants in water.

2.2 Ultraviolet band systems of molecular hydrogen

The hydrogen molecule is of fundamental interest, mainly because it is the simplest stable molecule and so accurate calculation of its electron structure can be performed. Also, molecular hydrogen lines are widely used as a calibration reference for VUV spectrum system. The Lyman-band system ($B^1\sum_u^+ \rightarrow X^1\sum_g^+$) and Werner-band system($C^1\prod_u^+ \rightarrow X^1\sum_g^+$) were first observed by

Lyman[60] and Werner[61] in the early twentieth century in the low resolution VUV emission spectra of molecular hydrogen[62]. Other pioneering investigations were also performed[63, 64]. Since that time, several investigations have been carried out at high resolution, with most of them quantifying absorption spectrum of molecular hydrogen[65-68]. Comparatively little was done in emission in the VUV region. The first high resolution emission study of Lyman bands was done by Herzberg and Howe[69]. Huber and Herzberg[59] summarized the work before 1980s and presented an extensive list of data reference. However, it was not until 1984 that the analysis was extended sown to 100nm by Dabrowski[70] for the Lyman and Werner bands. In the same period, Roncin et al.[71, 72] partly extended the analysis of the spectrum down to 78nm using a low-pressure discharge where self-absorption is much reduced at lower wavelength. In particular, they identified many bands of the ($C^1\prod_u^+ \rightarrow X^1\sum_g^+$) system. Elaborate emission studies were done by the Meudon group[73, 74] at higher resolution. Baig and Connerade[75] performd an absorption study on H_2 using synchrotron radiation. Meanwhile, Jungen et al.[76] determined the $B^1\Sigma^+_u$ state with v = 0 and v = 1 using Fourier-transform infrared spectroscopy. Amsterdam et al.[77, 78] performed extensive wavelength calibration studies on the Lyman bands of H_2, using a laser-based VUV source allowing for a much lower absolute uncertainty of transition frequency. Hollenstein et al.[79] and Philip et al.[80] presented the Lyman transition frequency calibrations.

From the theoretical point of view, the Morse representation of the $X^1\Sigma^+_g$ state and $B^1\Sigma^+_u$ state were given by Vanderslice et al.[81] and Tobias et al.[82] separately in the early 1960s. At the same time, Jarmain and Nicholls[83] provided an array of Franck-Condon factors of molecular hydrogen based on realistic Klein-Dunham potentials calculation[84]. In the mid-1970s, Julienne[85] and Ford[86] performed the first calculation of line emission probabilities of the Lyman and Werner Band systems of H_2, taking into consideration the rovibronic coupling between excited states. At that

time, however, no complete experimental high-resolution emission spectrum was available to check the calculations. Therefore, the comparison was passed over. A couple of refined calculations were performed in the following twenty years. Abgrall et al.[87] calculated the semi-ab-inotio emission probabilities and found very good agreement with intensity measurement. An extended list of oscillator strengths and level energies has been reported by Abgrall and Roueff[88]. Senn et al.[89] calculated level energies of the B and C states, up to J = 6 completely ab initio by including four excited states in the interaction. Abgrall and Roueff[62] later calculated an extensive line positions and emission probabilities of the Lyman and Werner band systems of molecular hydrogen by solving coupled Schrodinger equations.

2.3 UV phosphor study

Phosphor coatings have long been employed in the detection of UV radiation before customized VUV photon intensifier became commercially available. With the interest in the use of silicon charge coupled devices (CCD) imagers for deep VUV (120-160nm) detections, a UV sensitive phosphor is desired to match the VUV spectrum with the CCD sensitive spectrum region, which is usually above 350nm[5]. Three phosphors have been used for VUV detection, namely, Sodium Salicylate, Coronene and Liumogen. In this work, all of these material were studied and tested in our lab. From the preliminary results, Liumogen works the best at the incoming wavelength of 253.7nm (Mercury Lump), and the photon-efficiency of Coronene coating increases with thickness all the way to about 2000A. Further experiments and results are required to determine which one is the best in the working wavelength regime (120-160nm).

2.3.1 Sodium Salicylate

Sodium Salicylate is obtained as a very fine crystalline powder which can be dissolved in ethyl alcohol[6]. After forming a saturated solution, it is dripped to microscope slide using a standard dropper. The microscope slide is heated up by an electric heater with a constant temperature of about 600K. This temperature will significantly facilitate the evaporation of the alcohol while not high enough to make the evaporation process too intense to damage the coating.

The fluorescent efficiency appears to be independent of wave length from 584 to 2200 A. From the previous work at 1200 A, it can be seen from Fig. 2.1[6] that the efficiency rises rapidly to a maximum at 1 mg/cm^2 then falls off very slowly as the thickness increases[6]. A good application is to drip about 10 solution droplets uniformly to a 44 mm by 22 mm standard microscope slide for spectrometer usage which resulted in about 2mg/cm^2.

An improved method was applied following the idea proposed by R.A. Knapp[7]. A commercially available nebulizer for aerosol therapy is modified as shown in Fig. 2.2[7]. By dissolving the Sodium Salicylate powder in ethanol, the nebulizer is able to produce extremely fine mist. This mist is then directed through the exit onto the microscope slide to be coated. Since the mist dries immediately once contacting the surface, the coating may be applied continuously, and uniform layers of any desired thickness may be produced in a matter of minutes. However, in our application, the Sodium Salicylate coating is not as perfect as being proposed by Dr. Knapp. The deposition rate is extremely low, i.e. 0.01mg/cm^2/min, which takes at least one hour to have sufficient amount of deposition. Furthermore, the deposition is not as uniform as predicted. Due to the limited dimension and rate inconsistency of the exit mist, the microscope slide or the nebulizer has to be moved consistently to have the whole surface of the

slide uniformly covered by the mist, which is extremely tedious. In this particular experiment, the successful rate is even lower than the direct deposition method. Therefore, the direct deposition method is more favorable for sodium salicylate coating.

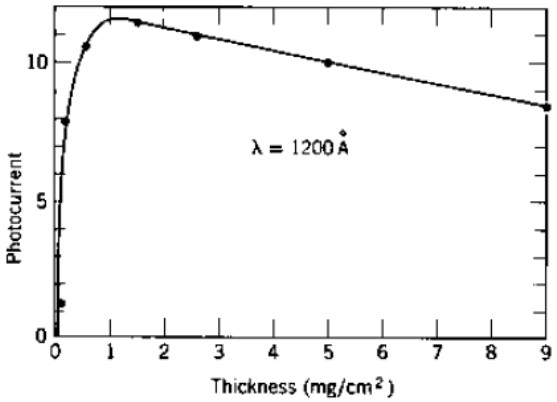

Figure 2.1 Relation between response and thickness of sodium salicylate layer at 1200 A[6].

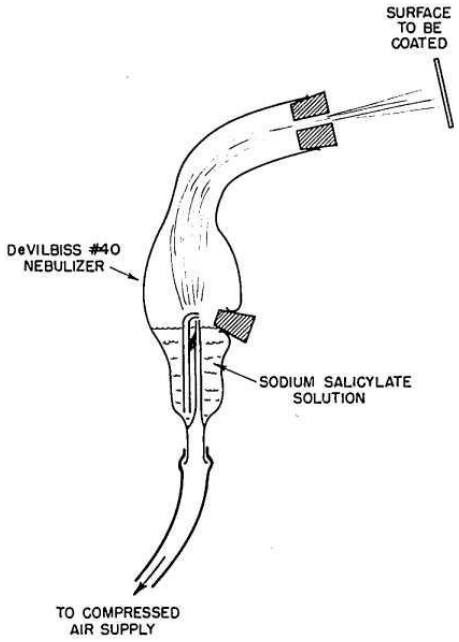

Figure 2.2 Nebulizer modified for preparing sodium salicylate layers[7].

2.3.2 Coronene Coating

Coronene coating has a higher fluorescent efficiency than Sodium Salicylate since its fluorescent emission intensity has a higher overlap with the CCD sensitive spectral response than that of Sodium Salicylate[5], as is shown in Fig. 2.3[5]. The sublimation temperature of Coronene[8] is around 200 ^{o}C and its density is 1.467g/cm^{3}. The best performance comes from the coating thickness from 500 to 2000 A. Another important issue to notice here is that Coronene is slightly toxic, so it is important to take some precaution such as wearing gloves and respirator.

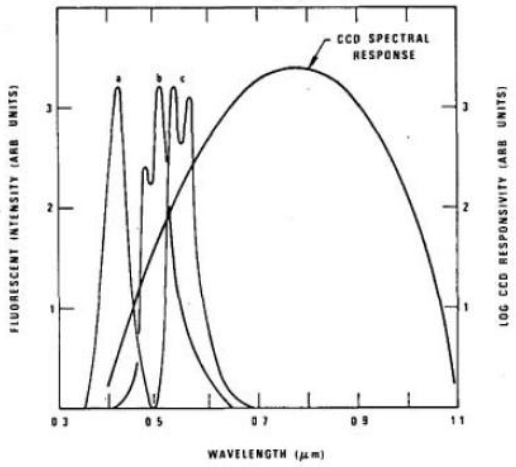

Figure 2.3 Fluorescent emission intensity as a function of wavelength for (a) sodium salicylate, (b) coronene, and (c) liumogen compared schematically with the spectral response of a rear illuminated Si CCD[5].

The Coronene coating is prepared by the standard vacuum evaporation process. The general procedure is attached in APP. 1. By comparison, the Coronene vacuum evaporation coating is yet the most mature and stable process. The thickness of the coating could be accurately controlled, and the coating is extremely uniform.

2.3.3 Liumogen

Liumogen has an even higher fluorescent efficiency than both Sodium Salicylate and Coronene due to its great overlap with the CCD sensitive spectral response[5]. And the results have shown that Liumogen works the best in converting 253nm photons into visible photons that could be detected by CCD detector. The preparation of Liumogen coating is quite straightforward. It is no more than just useing a yellow highlight marker to paint the slide and make sure that the slide is covered uniformly with highlight ink whose major component is Liumogen. The issue of Liumogen coating, however, is the aging problem. The photon converting efficiency could drop by a factor of five within twenty four hours. This is partially due to the method we are using here.

The composition of the highlighter ink is not specified. While it definitely contains Liumogen, it contains also various additional materials which present unknown function as VUV converter. Therefore, vacuum evaporation coating method is recommended for Liumogen coating just as has been reported by N. Kristianpoller[9].

2.3.4 Efficiency comparison

The mercury lump is used in this case to compare the photon converting efficiency of different coating. For sodium salicylate coating, coating thickness from 0.3mg/cm^2 to 1.5mg/cm^2 was tested. The photon converting efficiency, contrary to the result presented by earlier research[6], goes all the up as the coating gets thicker. The mercury lump is a broad band light source, while the earlier results came from narrow band 253.7 nm line. Studies by different groups[6, 10] have shown that sodium salicylate coating has various photon converting efficiencies with respect to different wavelength. A Coronene coating with the thickness ranging from 1000A to 2500A was tested. Results show that the photon converting efficiency increases as the thickness goes up. A 2500A coating yields the best efficiency. It is hard to quantitatively control the thickness of the Liumogen coating using the highlighter method, therefore only qualitative study was done here. Due to the significant aging issue as discussed above, Liumogen coating method is discarded in the experiment. The test results showed that, while both in their optimal efficiency thickness region, sodium salicylate coating generally yields higher photon converting efficiency compared with coronene coating by a factor of three. This is a bit counter intuitive since the fluorescent emission intensity of coronene has much higher overlap with the sensitive detective region of CCD camera than sodium salicylate. This issue is not yet completely addressed. One possible explanation is that the detector that we have been using here has a different sensitive wavelength

region behavior. Therefore, sodium salicylate is chosen as the UV converting phosphor in the experiment.

A comparison of the sodium salicylate UV photon converting efficiency with that of the photon intensifier is studied using the experimental setting discussed above. A first order calculation indicates that the coating, given perfect converting ratio, yields only 10% of the efficiency of the photon intensifier. Experimental data showed that the actual sodium salicylate efficiency is even worse than that. A three minutes exposure is enough for the photon intensifier to capture sufficient signal data to generate a clear spectrum; however, a half hour exposure yields nothing using the $1mg/cm^2$ sodium salicylate coated microscope slide. With the fact that researchers in the old days usually expose the phosphor and detector to the light sources for hours, it is reasonable that our weak UV source wouldn't yield any significant result using the phosphor with exposure time less than one hour. Longer exposure could be tested, however, with the UV photon intensifier at hand, phosphors are not favorable.

2.4 Impurities in vacuum systems and cleaning techniques

Gas handling in the vacuum system is important because extremely clean gases are needed for studying the excimer physics of rare gas light sourse[2]. It is suggested by Ulrich[2] that the gas cell should be pumped down to 10^{-6} mbar using a turbomolecular pump and baked at a temperature of 120^oC. Also the cell is to be flushed with pure gases from gas cylinders and filled. Additional gas cleaning includes an 800^oC electronically heated titanium wire to remove oxygen and nitrogen as well as zeolite to remove water vapor[2]. Therefore, a detailed review of the impurities involved in vacuum systems and cleaning techniques is presented as following.

2.4.1 General description of contaminants in vacuum system

Component parts intended for use in high vacuum systems must always be scrupulously clean. Visual examination is not adequate. Gases may be adsorbed on surfaces or absorbed in the interior of the vacuum components. As the pressure of a system is reduced to some certain level, this issue will become more important. In the first stage, the regular atmospheric gases will be pumped. When the pressure approaches the saturated vapor pressures of the contaminants in the system, the system pressure will drop much more slowly. The further pressure drop rate depends largely on the nature and property of the contaminants. The most common contaminant encountered in vacuum systems is water vapor, the saturated vapor pressure at room temperature and pressure is approximately 17 mm Hg. Other common contaminants include greases, oils, solder fluxes, etc., which are generally introduced in the fabricating or assembling process. The nature and property of contaminants will determine the time required to pump down to a particular pressure. The cleaning methods to be considered should make it feasible to pump the system down to a certain vacuum level, usually 10^{-6} mm Hg within reasonable time scale. Different vacuum level requires different combination of cleaning techniques and operating procedure.

Guthrie suggested a reasonable method of classifying the various types of contamination, which is the following:

a. Visible contaminants such as deposits of tapping compounds, cutting oil, polishing materials, varnish, etc.

b. Contaminants hidden in crevices and holes.

c. Gases and vapors adsorbed on surfaces.

d. Gases and vapors absorbed/dissolved within vacuum materials.

e. Gases and vapors which are combined chemically with materials of the systems.

As a rule of thumb, the type a and b contaminants should be cleaned up in all of the vacuum systems, which is relatively simple. However, more effort should be expended to eliminate the other types of contaminants where higher vacuum is desired, i.e. lower than 10^{-6} mm Hg, or when attenuation should be minimized.

2.4.2 Gas releasing mechanisms and material outgassing properties

Gases are dissolved in and adsorbed on solid surfaces. Those gases will release in vacuum systems as a result of several factors, namely, vaporization, thermal desorption, diffusion, permeation and stimulated desorption. The term describing the general gas releasing process is referred to as outgassing.

The maximum vaporization rate of a solid could be calculated using the following equation:

$$\Gamma(molecules/s) = 2.63 \times 10^{24} \times \frac{PA}{(MT)^{0.5}} \qquad (2.1)$$

Where the P is the vapor pressure, A is surface area, M is molecular weight and T is temperature.

The diffusion rate could be found by applying Fick's law and solving the differential equation of mass transport which may be an involved calculation for some systems. A good description could be found in O'Hanlon[12].

The desorption and permeation mechanism are much more complicated and therefore are beyond the purpose of this discussion; however, a good review of the above mechanisms could be found in O'Hanlon[12].

2.4.2.1 Metals

Metals are the most widely used material in vacuum system. They should have high strength, low permeability to atmosphere gases, low outgassing rate and low vapor pressure. Most metals have sufficiently low vapor pressure. Some materials, however, have high enough vapor pressure and could interfere with normal baking procedure. Alloys containing zinc, lead, cadmium, selenium and sulfur should be used with great care. The vapor pressure of common metals could be found in Appendix C.6 and Appendix C.7 of O'Hanlon[12].

The permeability issue of gases in a metal is usually negligible with the only exception being hydrogen. The permeation rate of hydrogen is proportional to the square root of the pressure difference. The permeation constant of hydrogen through various metals as a function of temperature is found in Fig. 16.1 of O'Hanlon[12].

The gas load in vacuum systems is adsorbed and dissolved in metals. Gas is dissolved in a metal during the initial melting and casting. It consists mainly of hydrogen, oxygen, nitrogen and carbon oxides. Gas is also physisorbed and chemisorbed on the interior surfaces from exposure to ambient atmosphere. It consists of mainly water vapor, with carbon oxides, oxygen and nitrogen. The SI outgassing rate has units of Pa-m/s and the pressure in a chamber with net outgassing rate (q), area (A) and pump speed (S) could be calculated using the following equation:

$$P(Pa) = 1000\,\frac{q(Pa-m/s)A(m^2)}{S(L/s)} \tag{2.2}$$

Vacuum firing of components will effectively remove the dissolved gas load in cleaned and degreased parts. Hydrogen firing is traditionally used for this purpose, because it reduces surface oxides. However, the drawback comes from its relatively higher permeability. Vacuum or inert gas firing is preferred for vacuum systems especially for ultrahigh vacuum systems. The maximum firing temperatures for several metals are given in Table 16.1 of O'Hanlon. For example, the maximum firing temperature is 500°C for copper and alloys, and 1000°C for stainless steel. Based on a single diffusion constant model proposed by W. A. Rogers[15], the time to depletion is $t = d^2/(6D)$ and a 1 hour baking at 1000°C is equivalent to 2500 hours of baking at 300°C.

2.4.2.2 Other Materials

Materials other than metals that are commonly used in vacuum systems are glasses, ceramics and polymers. The gas on the surface of glass is primarily water with some carbon dioxide. A high temperature baking of glass could completely eliminate outgassing of water from glass, because all the surface water is released in a high temperature bake and the diffusion constant of water vapor is negligible at room temperature. The outgassing of polymer materials is dominated again by the evolution of water vapor. This gas load could also be reduced by baking. Something to keep in mind is that at higher temperature, polymers begin to decompose; for example, Kalrez can withstand temperatures up to only 275°C.

2.4.3 General cleaning methods

The first step is to remove as much gross contamination as possible by mechanical means, such as blasting with abrasives and rubbing with emery cloth. Filings and small loose particles can be removed by using air hose. Due to the fragile nature of some vacuum components such as filaments, the usage of mechanical cleaning methods is limited. Also, ceramics and glasses should be wiped with a clean, lint-free cloth as a preliminary step. An air supply is useful in the cleaning procedure. However, the supply should be equipped with satisfactory oil filter to minimized oil contamination.

The following steps are generally considered as adequate for various vacuum systems.

1. Clean with a soap solution or synthetic detergent.
2. Rinse with hot distilled water. The first two steps are to eliminate gross contamination.
3. Rinse in a suitable solvent. Acetone, methyl ethyl ketone and methyl alcohol are most commonly used. This step is to dissolve paints, vanishes and to some extent, water.
4. Use a vapor degreaser with a chlorinated solvent. Trichloroethylene is generally used due to its low toxicity.
5. Rinse in two changes of methyl alcohol or acetone.
6. Dry in warm air blast or oven at 70^{o}C to $110\ ^{o}$C.

These six steps are enough to eliminate the types a and b contaminations discussed in section 2.4.1. Usually those steps are carried out prior to the assembly of the systems or incorporation of new components. One precaution is that parts cleaned according to the above directions should

not be left exposed longer than necessary to the atmosphere. Try to store clean components and parts in a dry and dust-free environment if necessary.

To cut down the time required to reach an operating pressure, attention must be given to reducing contaminants c, d and e mentioned in section 2.4.1. Type c contaminant is primarily water due to the exposure to the atmosphere. To speed up the vaporization of the water, the procedure is to heat surfaces. This is best done in vacuum and can be carried out by either incorporating a heat cycle into a preparatory phase of the pump-down or using a separate system. The transfer time should be kept at minimum if a separate system is required. If parts must be heated in air, then this should be done in an oven. The temperature should be raised above the boiling temperature of water, which is 100^{o}C at atmosphere pressure. The temperature must be lower than the firing limit discussed in section 2.4.2.

Removal of contaminant of type d again involves the use of heat but for longer time this time, in order that the absorbed gases and vapors can diffuse to the surface and be pumped away. Higher temperature could facilitate the procedure but again the temperature should be maintained below the material limit.

In most cases oxides and other chemical compounds, the last type of contaminant, are removed by chemical or electronic means. It must be kept in mind that many vacuum materials such as stainless steel and aluminum can be used without the removal of the oxide layers because their vapor pressure is negligible. Ultrasonic cleaning could be used to clean the non-negligible oxide layers, such as the rusty iron.

More detailed description of cleaning of metals and other material could be found in chapter 7.2 of Roth[11].

2.4.4 Gas impurities in liquid gas source

Argon is used here as the excimer gas source, while krypton is used as a control group. Both commercial grades and ultrahigh purity argon gas were used in this study. The commercial grades argon was used to replicate the study of Murnick group[2], while the ultrahigh purity argon was tested to compare the effect of gas impurity.

The purity level of commercial grades argon varies from 99.7% to 99.9%. The principal contaminant is nitrogen, plus about 0.001% hydrogen and 0.001% oxygen[17]. Various argon purification methods could be applied to increase the argon purity up to three orders of magnitude. Gettering materials such as uranium[18] and titanium[17] were tested and the results were satisfactory. The only remaining active gas will be hydrogen which is released in the reaction between water vapor, hydrocarbons and gettering materials. However, the hydrogen impurity level is around 0.001% and can be tolerated in most of the applications. The commercial grade argon gas used here is not further purified, and the expected impurity level is somewhere between 0.1% and 0.3%.

Ultrahigh purity argon has a very high purity level. The parameter used here to determine the impurity level is known as the oxygen equivalent. For ultrahigh purity argon, the oxygen equivalent should be less than 0.1 ppb. The most common purification method of liquid noble gases is the electron capture mechanism and was reported by several different groups[19,20,21]. The main difference amongst those experiments is the method of production of free electrons in the liquids[19]. The 0.1 ppb level of impurity could be safely neglected and serves good as a control pure gas source.

2.5 Electron energy loss passing through the membrane

For light particles such as electrons penetrating a solid, the energetic particles lose energy primarily through excitation and ionization in inelastic collisions with atomic electrons, termed as "electronic-energy loss." Microscopically, energy loss due to excitation and ionization is a discrete process. Macroscopically, however, it is a good assumption that the moving ions lose energy continuously. All we are concerned with here is the average energy loss during the penetration of electrons into a given material[23].

To measure energy loss, we must determine two quantities: the distance Δt that the electrons traverse in the target, and the energy loss ΔE in this distance. The mass density ρ or the atomic density N are frequently combined with the distance, in the form $\rho\,\Delta t$ or $N\,\Delta t$, to express the amount of material per unit area or the number of atoms per unit area that the projectiles have traversed in losing energy ΔE to the target material. Energy loss can be expressed in several different ways. Some frequently used units are[23]:

$$dE/dx: \text{eV/Å} \tag{2.3}$$

$$(1/\rho)\, dE/dx: \text{eV}/(\mu\text{g/cm}^2) \tag{2.4}$$

$$\text{Stopping cross section } \varepsilon = (1/N)\, dE/dx: \text{eV}/(\text{atoms/cm}^2),\ \text{eV cm}^2 \tag{2.5}$$

$$\text{Stopping power } L = \text{MeV cm}^2/\text{g} \tag{2.6}$$

Tables of range and stopping power of electrons which include data for 10keV can be used to estimate the energy loss of the electrons in the entrance window[2]. For 20keV electrons in SiN_x foils, stopping power data could be obtained from a tabulated value of about 10 MeV cm^2/g for

aluminum[22], which is similar in atomic number and density to silicon. Using this value, the energy loss is only 0.75keV in a 300nm thick silicon nitride entrance foil, which is less than 4%.

The characteristic parameters used in this experiment are 12.5keV electrons and 150 nm SiN_x foils. 12.5keV electrons will result in more energy loss compared with 20ekV electrons, while the thinner foil will decrease the energy loss. These two effects counterbalance each and the estimated energy loss would be close to that obtained using a combination of 20keV and 300nm silicon nitride foil, which is approximately 4%-5%.

2.6 Electron beam penetration in the test gas

Energy loss and angular scattering processes have to be considered for the energy deposition of an electron beam in a gas target. Stopping and energy deposition of low energy electrons in solid and gaseous matters has been studied extensively[2]. The Monte Carlo method was primarily used in those studies to get the spatial distribution of the energy deposited by electrons in different matters. Valkealahti et al. used Monte Carlo simulation method to investigate the spatial distribution of deposited energy for 1-10keV electrons incident on solid hydrogen, nitrogen, neon, silicon, aluminum and argon[25]. Berger and Seltzer computed the distribution of 2-10keV electrons incident on atmosphere air[31]. The transport of electrons in molecular nitrogen and air has been studied in the energy range between 5keV and 50keV using the Monte Carlo method and simulating the trajectories of the electrons directly from elastic and inelastic cross-section avoiding the continuous slowing down approximation and multiple scattering theories[29]. Monte Carlo and continuous slowdown approximation approaches to the spatial deposition of energy on hydrogen by electrons energy up to 2keV are compared using the detailed atomic cross section[27,

[28]. Vasenkov computed the energy and space dependent electron flux for 0.1-10keV incident electrons in argon using also the Monte Carlo method[32].

Experimental measurement was also done by different groups. Grün has measured, in air, the distribution of the total radiation emission from planes perpendicular to the initial beam direction, as a function of axial distances from the gun[33]. Cohn measured the side-view intensity profiles of nitrogen radiation emission caused by an electron beam with energy between 2-5keV[24].

Detailed theory of electron penetration in an infinite medium under the combined influence of scattering and slowing down was well presented by Spencer[30]. The energy deposition along the individual tracks of electrons is described by the well-known Bethe formula[35]. Large angle scattering, however, reduces the penetration depth of the electrons measured along the initial direction of the electron beam, A characteristic plume of excited matter is formed around the spot where a well collimated beam if electrons is sent into a target material. The plume size could be quantified by using "practical range" suggested by Schumacher[34]. Grün found that his measurement of practical range L over the energy range of 5-50keV can be accurately fit by the simple relation: $L = 2.60E^{7/4}/\rho\ cm$, where E is in keV and ρ in Torr[35]. In the continuous slowdown approximation[24], the path length is given by $l = \int_0^E dE/(dE/ds)$, substituting $\rho/E^{3/4}$for dE/ds, we find that the CSDA path is proportional to $E^{7/4}/\rho$. The numerical CSDA path length presented by Berger[22] could be fit accurately by $L = 2.95E^{7/4}/\rho\ cm$.

Energy deposition along the original direction of the beam and integrated perpendicular to the beam leads to a characteristic profile which can be approximated by a Gaussian Function[25]. Energy deposition of 7, 2, 1, 0.7 and 0.5mm for He, Ne, Ar, Kr and Xe, respectively are obtained for 15keV electrons and a gas pressure of 1 bar using tabulated ranges from Berger[2, 22].

2.7 Attenuation in the VUV spectrometer

The degree of vacuum necessary in a spectrograph to prevent any appreciable attenuation of the radiation from the light source depends on the wavelength and the path length from the entrance slit to the plate holder via the diffraction grating. The amount of attenuation of the radiation is given by the Lambert-beer law, namely[36],

$$I = I_0 e^{-\sigma n L} \tag{2.7}$$

Where I_0 is the intensity of the unattenuated beam while I is the intensity reaching the plate holder or the exit slit; the path length traveled by the radiation is L; the number of molecules in the spectrograph is represented by n per cubic centimeter, and the absorption cross section of the molecule (air) is represented by σ, or[37],

$$I = I_0 e^{-kL} \tag{2.8}$$

where k is the absorption coefficient and $k = \sigma n$. The absorption cross section and absorption coefficient of a gas are functions of wavelength and in general are greater at wavelength short than the first ionization potential of the gas. Since the first ionization of most gases lie below 1100 Å, and no window materials exist below 1040 Å, the minimum vacuum requirements are divided naturally into two regions above and below 1100 Å. The region below 1100 Å not only requires a better ultimate vacuum than the region above 1100 Å, but it also requires higher pumping speeds and remove the gas, which continuously diffuses in through the entrance slit from the light source. Pressure of 10^{-4} to 10^{-6} torr are quite adequate for most vacuum spectrographs and monochromators[36].

The absorption coefficients of nitrogen and oxygen in ultraviolet region are well studied by Watanabe[37]. As suggested by Watanabe, there exists no nitrogen absorption continuum in the region of 850-1450 Å and the dominant radiation absorption that leads to the signal attenuation stems from oxygen absorption. The most significant oxygen absorption continuum in the region of 1200 Å to 1900 Å is the Schumann-Runge continuum[38-42]. From the study of Allison et al.[39], Ackerman et al.[40] and Yoshino et al.[41], the absorption cross section of molecular oxygen is well below 10^{-17} cm^2. It is fairly straightforward to find relationship between the attenuation and air pressure using the Lambert-beer equation for any given cross sections. The air pressure is related with the total molecular density through the idea gas law. The relationship graph is given below. As is obviously illustrated in the graph, signal attenuation could be kept less than 10% for an optical length of 1 meter if we could maintain the spectrograph pressure of less than 0.01 torr.

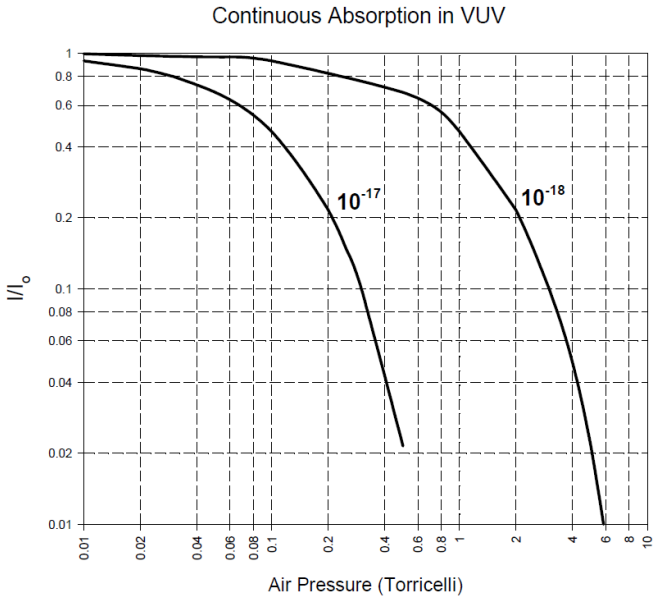

Figure 2.4 the signal attenuation with respect to gas pressure at different given cross section (path length is 1.1m)

3. Experiment

3.1 Experimental Setup

The experiment layout has three basic components: source, spectrometer, and detector, as shown in the figure 3.1 below:

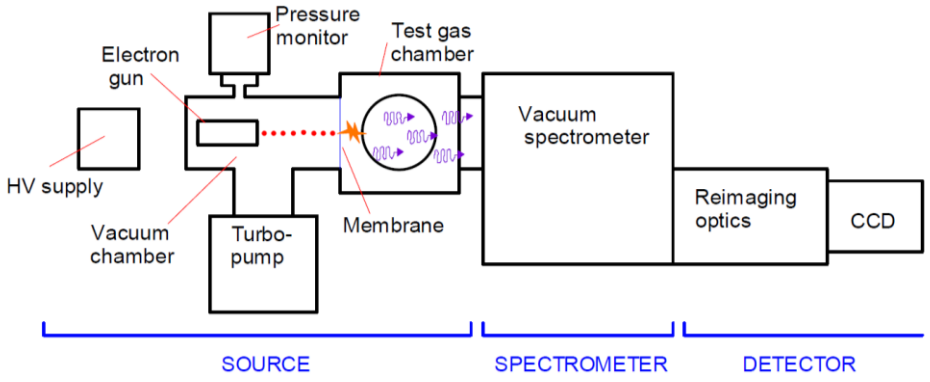

Figure 3.1 The experiment overview

The source generates the UV light we want to analyze. It's basically a high vacuum chamber with an electron flooding tungsten filament, which could generate hot electrons provided with a 6V direct current power supply. These electrons are then accelerated by a dc voltage of approximately 12.5 kV between the filament and a vacuum flange. A 150nm SiN_x membrane glued to a 1mm diameter aperture on a copper gasket lets the electrons pass into a chamber that holds the test gas without significant energy loss. The test gas is excited by the electrons in a controllable gas mixing chamber, emitting UV light.

The high vacuum region has been pumped down to 10^{-5} mbar using a Pfeiffer HighCube 80 Eco two stage pumping station. The pumping station basically is the combination of a diaphragm backing pump and a high vacuum turbo pump. It takes about 30 minutes for this pumping system

to generate vacuum lower than 10^{-5} mbar. The pressure is monitored here using an Edwards Active Inverted Magnetron gauge. The measurement range of this gauge is $1x10^{-9}$ to $1x10^{-2}$ mbar. All of the parts in the source part are flange connected in order to minimize leakage. The electrical circuit is formed by a tunable 15 kV Acopian N015HA2 high voltage power supply with positive terminal grounded and negative terminal connected with the filament cathode. The hot electrons are generated on the filament which is powered by isolated 6V batteries. An alternative electron gun design has also been applied and tested following the study of William Parker[3]. However, this method is relatively unstable, and an issue has been brought up previously concerning the potential burning through of the diaphragm due to the relatively higher electron power and density. The concept of using SiN_x membrane for low energy electrons windows was first introduced by Hanlon, and later successfully applied by Murnick[1] and Mills[4]. A simple method of preparing the SiN_x membrane is presented by Murnick[1]. The commercially available SiN_x membrane significantly facilitates the experiment process. The 1mm and 0.5mm square SiN_x membrane with thickness of 100nm, 150nm and 200nm were tested here. The thinner diaphragm tends to decrease the electron energy loss upon passing through but at the same time bares a much higher risk of breaking down during operation. Since the replacing of the diaphragm is tedious, a combination of 0.5mm square with 150nm was used in this experiment and yielded satisfactory result. The diaphragm is glued to the standard copper gasket using high vacuum epoxy and then the gasket is secured between two flanges. The gasket as well as the SiN_x membrane together act as the barrier between the high vacuum chamber and the testing gas chamber.

The hot electron flood generated at the filament is significantly accelerated by the imposed 12.5 kV dc voltage. Most of the electrons will hit the gasket and dissipate to the ground, but a small portion of the electrons will pass through the SiN_x membrane. Dr. Richard Miles brought up the issue of the electron energy loss when passing through the membrane as well as the electron penetration depth in the gas chamber in a seminar meeting at UIUC. These issues were not fully addressed in this work. The passed electrons then interact with the gases in the test gas chamber and generating light. The test gas chamber is basically is a flange tube with inlet and outlet tube connection. The inlet and outlet connections are connected with the test gases stored in the steel cylinders as well as appropriate gauges.

The light is transmitted through an MgF_2 window and then enters into the VUV spectrometer. The VUV spectrometer is custom designed. Basically it is made up of two MgF_2 coated aluminum mirrors, a grating and a VUV photon intensifier, a VUV interference filter centered at wavelength 150nm with FWHM of 60nm. The VUV spectrometer is pumped down to and maintained at 0.1 mbar using a diaphragm pump. The VUV photons are further reimaged optically and focused on to the Andor DU420A-BU scientific high sensitivity CCD camera. Progressive sensitivity and spectrum calibration has been performed using Mercury lamp at 253 nm and 185 nm spectrum without and with the UV filter respectively. The completely assembled experimental setting could be seen in figure 3.2.

VUV spectrometer with filter and intensifier inside

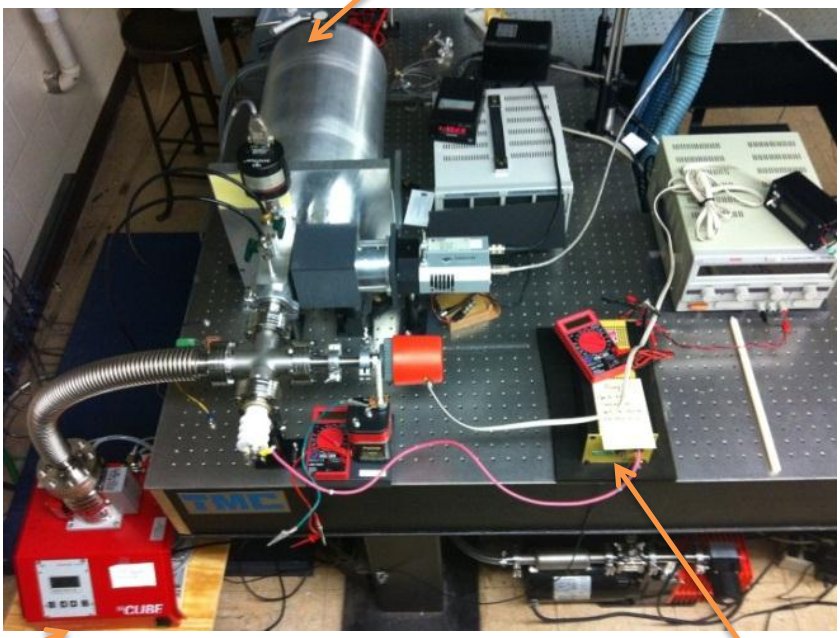

High Vacuum Turbo Pump

15kV HV supply

Figure 3.2(a) Experimental Setting

Reimaging Optics

CCD Camera

AMG high Vacuum Gauge

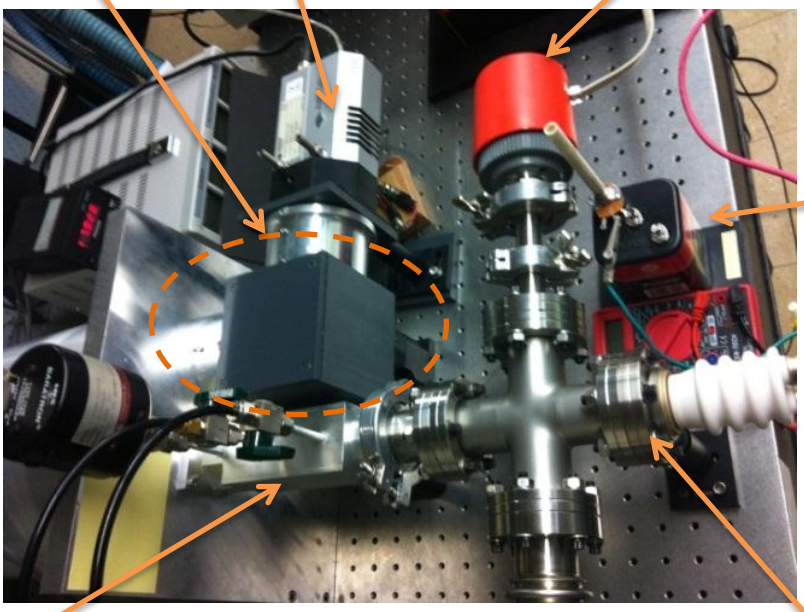

Isolated Power supply

Test Gas Chamber

Electron Flooding Source

Figure 3.2(b) Experimental Setting

3.2 Calibration using H_2 Lyman bands feature

Emission lines of molecular hydrogen in the electron impact excimer system were used to calibrate the system. The test gas used here is argon with 3% molecular hydrogen. The test gas pressure was 800 torr and accelerating electric difference was 15kV. The spectrum within the region of 150nm and 170nm is given in Fig. 3.3. The experimental data will later be compared with simulated data to calibrate the system. The rovibronic spectrum of molecular hydrogen is calculated using the Diatomic program. Diatomic automatically calculates the rotational emission lines given appropriate molecular constants and vibrational bands. In order to gain some confidence about the Diatomic program results, code was made using spreadsheet following the well-known polynomial energy level calculation equation as follows[59].

$$\mathrm{G}(v) = \omega_e\left(v+\frac{1}{2}\right) - \omega_e x_e\left(v+\frac{1}{2}\right)^2 + \omega_e y_e\left(v+\frac{1}{2}\right)^3 + \omega_e z_e\left(v+\frac{1}{2}\right)^4 \tag{3.1}$$

$$F_v(J) = B_v J(J+1) - D_v J^2(J+1)^2 + H_v J^3(J+1)^3 + \cdots \tag{3.2}$$

$$B_v = B_e - \alpha_e\left(v+\frac{1}{2}\right) + \gamma_e\left(v+\frac{1}{2}\right)^2 + \cdots \tag{3.3}$$

$$D_v = D_e + \beta_e\left(v+\frac{1}{2}\right) + \cdots \tag{3.4}$$

The calculated line positions using spreadsheet and using Diatomic show a very good agreement. Two sources of molecular constants of molecular hydrogen Lyman bands were tested and compared, Herzberg and Howe[69] (1959) and Dabrowski[70] (1984). The molecular constants were polynomially fitted using the tabulated vibrational and rotational energies[70] and the result was very close with that fitted by Dabrowski. Emission line positions were calculated using both Herzberg and Howe and Dabrowski constants, and the results were compared with the more

recently published tabulated line position[73]. Although both sets of constants seem to deviate from the tabulated line position as vibrational quantum number v and rotational quantum number J increase, Dabrowski constants simulation only generate a trivial deviation, i.e. less than one tenth wavenumber when v and J are below 5. On the other hand, the smallest deviation using Herzberg and Howe constants are on the order of wavenumbers. Therefore, Dabrowski constants were applied in all of the spectrum simulations. The Dabrowski constants are given in table 3.1. Franck-Condon factors for H_2 Lyman system are from Nicholls table[83] and are given in table 3.2. The typical operating interface of Diatomic is shown in figure 3.3(a) and (b). Rotational temperature was set as 300K and Vibrational temperature was set as 10,000K which is reasonable input numbers for electron impact excimer systems. Centrifugal distortion constants, spin-orbit splitting constants, spin-rotation splitting constants and spin-spin splitting constants are not available for molecular hydrogen and therefore were set as zero. Twelve Lyman vibrational bands were selected which overlap the 158 to 162nm region, namely, *0-8, 1-9, 2-9, 2-10, 3-10, 4-11, 5-11, 5-12, 6-12, 6-13, 7-13* and *7-14* band. The complete simulation results, including the line position, strength and etc. are given in appendix 1. The simulated spectrum is given as figure 3.5.

TABLE 15. Equilibrium constants of the $X\ ^1\Sigma_g^+$, $B\ ^1\Sigma_u^+$, and $C\ ^1\Pi_u$ states of H_2

Y_{ik}	$X\ ^1\Sigma_g^+$ (cm^{-1}) 6 level fit	$B\ ^1\Sigma_u^+$ (cm^{-1}) 7 level fit	$C\ ^1\Pi_u^-$ (cm^{-1}) 5 level fit
$Y_{01}(\approx B_e)$	60.8468 (32)*	19.984 (17)	31.324 (18)
$Y_{11}(\approx -\alpha_e)$	−3.0525 (47)	−1.115 (21)	−1.599 (17)
Y_{21}	0.0502 (18)	0.0836 (71)	0.0135 (34)
Y_{31}	−0.0038 (2)	−0.0044 (67)	
$Y_{02}(\approx D_e)$	0.04644 (7)	0.01656 (18)	0.01994 (38)
Y_{12}	−0.00184 (6)	−0.00208 (12)	−0.00053 (13)
Y_{22}	0.00007 (1)	0.00013 (2)	
$Y_{03}(\approx H_e)\times 10^5$	4.57 (6)	1.50 (8)	
$Y_{13}\times 10^5$	−0.17 (2)	−0.19 (2)	
$Y_{04}(\approx L_e)\times 10^8$	3.56 (15)		
$Y_{14}\times 10^8$	−0.14 (4)		
$Y_{10}(\approx \omega_e)$	4402.93 (11)	1357.19 (12)	2444.66 (29)
$Y_{20}(\approx -\omega_e x_e)$	−123.07 (9)	−20.15 (10)	−68.58 (29)
$Y_{30}(\approx \omega_e y_e)$	1.46 (3)	0.46 (4)	0.36 (6)
$Y_{40}(\approx \omega_e z_e)$	−0.080 (3)	−0.021 (3)	
Y_{00}	8.42	8.26	4.54
$G(0)$	2170.88	673.61	1205.23
$E(0)$	2179.30	681.87	1209.77

*The numbers in brackets refer to the standard deviation of the last digits.

Table 3.1 Molecular constants of molecular hydrogen provided by Dabrowski[70].

TABLE 2

FRANCK-CONDON FACTORS FOR THE LYMAN-BAND SYSTEM OF H_2*

v′	v″ 0	1	2	3	4	5	6	7	8	9	10	11	12	13	14
0	6.6591 (3)	3 4638 (2)	9 7418 (2)	**1.8128 (1)**	**2.3778 (1)**	**2.2171 (1)**	1.4343 (1)	6.0595 (2)	1.4849 (2)	1.6327 (3)	3 4240 (5)	7.8637 (7)	1.0933 (8)	8.7627 (9)	1.4492 (9)
1	2.9411 (2)	9 6317 (2)	**1.4917 (1)**	1.0874 (1)	1.6143 (2)	2.4234 (2)	**1.5425 (1)**	**2.2544 (1)**	1.4812 (1)	4.3971 (2)	4.2191 (3)	1.1192 (5)	8.2453 (6)	3.3865 (7)	6.0758 (2)
2	6.8452 (2)	**1.2927 (1)**	8.4856 (2)	2.9243 (3)	4.6972 (2)	**1.0657 (1)**	2.6868 (2)	3.1562 (2)	**2.0416 (1)**	**2.1983 (1)**	7.3845 (2)	4.6491 (3)	6.9523 (5)	7.1421 (6)	3 7255 (6)
3	1.1161 (1)	1.0448 (1)	1.1082 (2)	3.2256 (2)	**7.9801 (2)**	9.0630 (3)	4.5296 (2)	**9 1224 (2)**	3.6450 (4)	1.5167 (1)	**2.7132 (1)**	8.9715 (2)	1.6153 (3)	5.3379 (4)	1.9733 (5)
4	1.4300 (1)	4.8687 (2)	6.3688 (3)	**6.9933 (2)**	1.7302 (2)	2.6627 (2)	**6.4734 (2)**	1.4983 (4)	**8.7779 (2)**	2.0932 (2)	1.1869 (1)	3.1625 (1)	7.8410 (2)	4.1542 (4)	4.8588 (4)
5	**1.5310 (1)**	7.1763 (3)	4.0555 (2)	4.3375 (2)	4.7846 (3)	**5.7968 (2)**	2.8818 (3)	**5.4281 (2)**	1.9556 (2)	**5.2591 (2)**	4.0581 (2)	1.2251 (1)	**3.5613 (1)**	3.6037 (2)	7.9543 (3)
6	1.4222 (1)	2.7527 (3)	**5.6642 (2)**	5.9567 (3)	3.8762 (2)	2.1543 (2)	2.1092 (2)	3.6730 (2)	1.5787 (2)	4.5711 (2)	2.5789 (2)	4.1401 (2)	1.7895 (1)	**3.5116 (1)**	1.2318 (4)
7	1.1746 (1)	2.8134 (2)	4.0038 (2)	3.3675 (3)	**4.5906 (2)**	1.5320 (4)	**4.3657 (2)**	1.6256 (4)	**4.8173 (2)**	2.3902 (4)	**5.3407 (2)**	1.3517 (2)	2.2766 (2)	3.1344 (1)	2.1972 (1)
8	8.7664 (2)	6.2067 (2)	1.3046 (2)	2.2686 (2)	2.1409 (2)	1.9560 (2)	2.0244 (2)	1.9156 (2)	1.6923 (2)	3.2077 (2)	3.6682 (3)	**4.8907 (2)**	9 4039 (3)	4.1445 (4)	**4.8697 (1)**
9	5.9737 (2)	8.6632 (2)	8.8447 (5)	**3.3674 (2)**	1.7383 (3)	**3.6505 (2)**	2.8094 (4)	**3.3536 (2)**	5.3914 (4)	**3.2337 (2)**	1.4243 (2)	9 6269 (3)	**4.1545 (2)**	6.2442 (3)	4.6135 (2)
10	3.7363 (2)	**9 4535 (2)**	8.2780 (3)	2.6263 (2)	3.1274 (3)	2.8540 (2)	9 4186 (3)	1.7071 (2)	1.7884 (2)	5.1517 (3)	**3.2298 (2)**	4.8943 (3)	1.1039 (2)	**3.6508 (2)**	3.8610 (5)
11	2.1452 (2)	8.7571 (2)	2.9671 (2)	1.0673 (2)	1.4479 (2)	1.0302 (2)	2.5719 (2)	9 7583 (4)	**2.5743 (2)**	2.6540 (3)	1.5631 (2)	**2.4742 (2)**	1.7345 (3)	7.6844 (3)	**4.1921 (2)**
12	1.1232 (2)	7.1759 (2)	5.1972 (2)	7.2105 (4)	**2.0556 (2)**	4.4117 (4)	**2.7943 (2)**	4.2692 (3)	1.3561 (2)	1.6251 (2)	4.3838 (4)	2.0367 (2)	1.7544 (2)	1.1077 (3)	1.4892 (3)
13	5.2715 (3)	5.3233 (2)	**6.6523 (2)**	2.5731 (3)	1.6822 (2)	2.3110 (3)	1.7345 (2)	**1.6701 (2)**	1.4224 (3)	**1.9422 (2)**	4.9927 (3)	4.4888 (3)	**1.9414 (2)**	**1.3037 (2)**	1.1127 (3)

* Entries for locally strong bands are set in boldface type. The number in parentheses after each entry is the negative power of ten by which that entry is multiplied.

Table 3.2 Franck-Condon factors of Lyman-band system of molecular hydrogen by Nicholls[83].

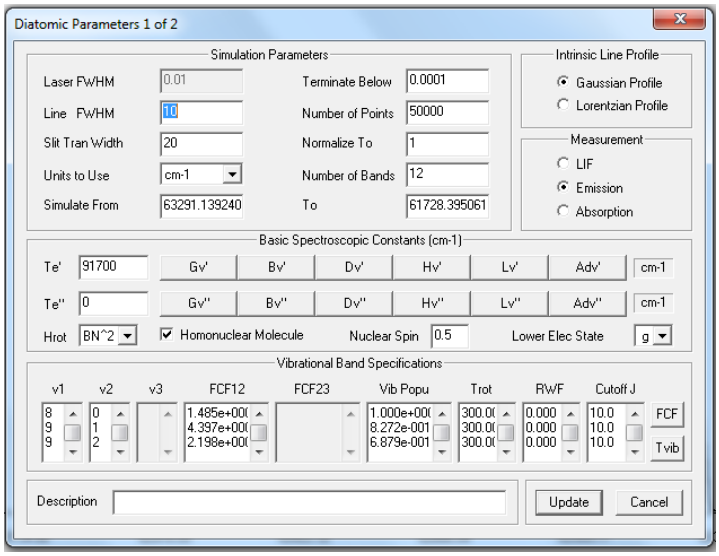

Figure 3.3(a) Diatomic constants input interface (a)

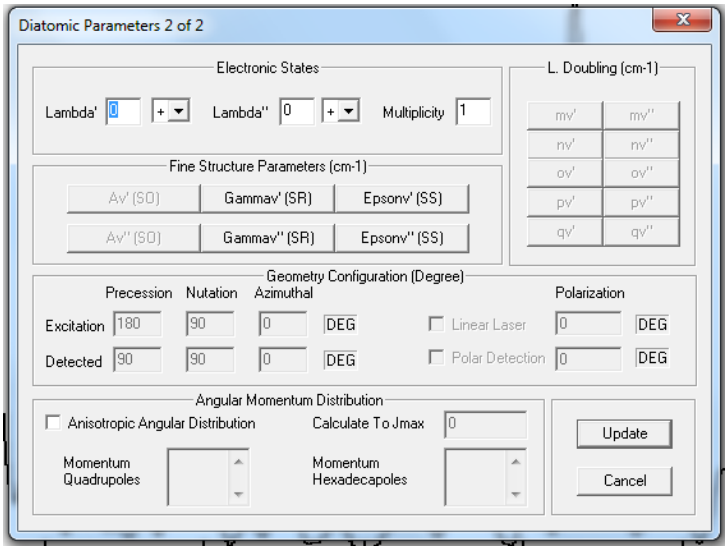

Figure 3.3(b) Diatomic constants input interface (b)

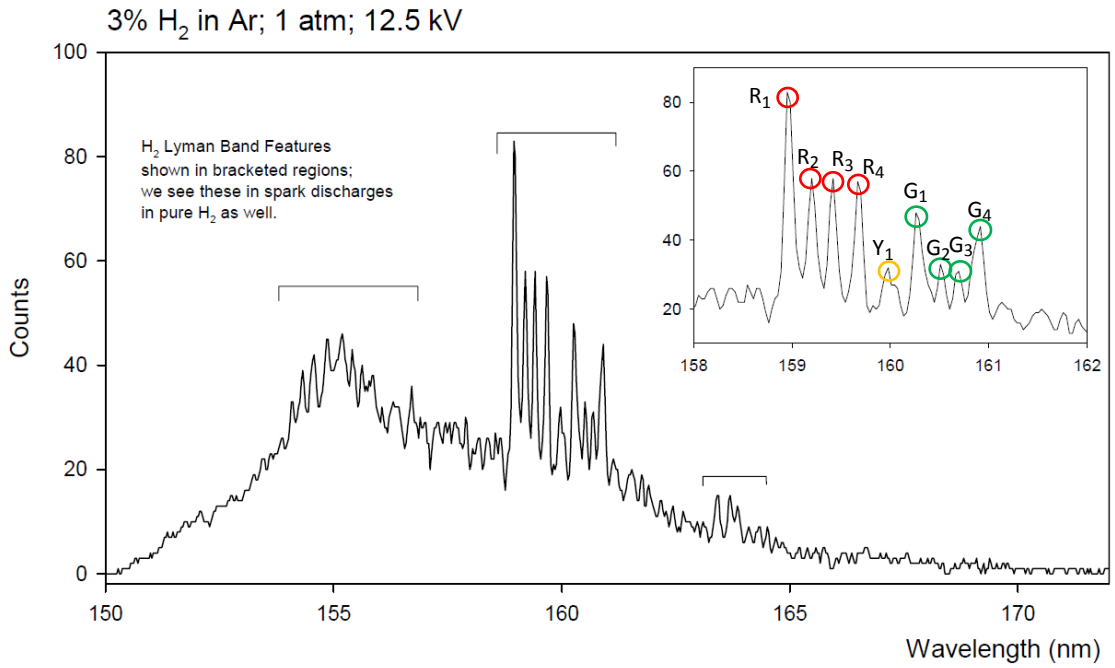

Figure 3.4 argon and H_2 (3%) excimer spectrum in the region between 150 and 170nm, higher resolution spectrum is on the up right.

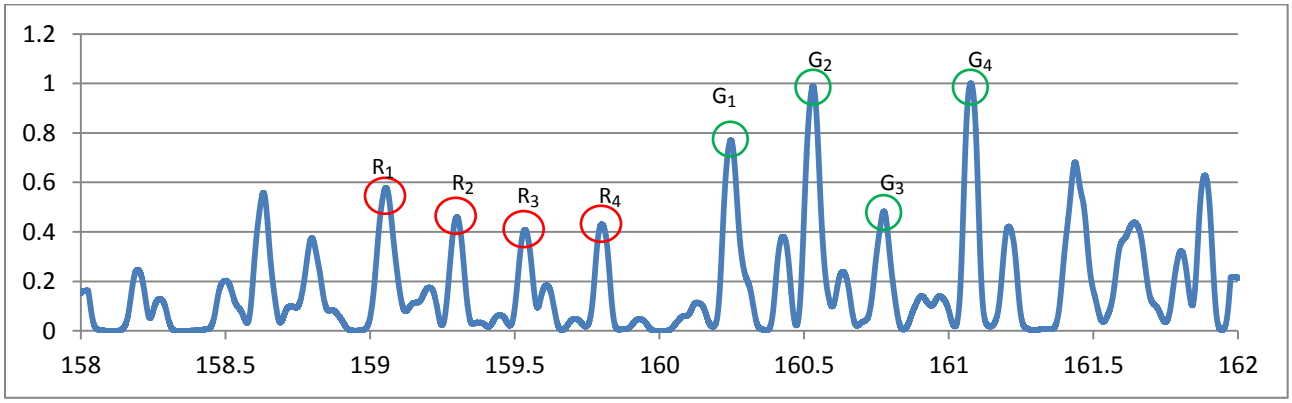

Figure 3.5 Simulated spectrum of molecular hydrogen emission lines using Diatomic program.

The experimentally collected spectrum figure 3.4 and the Diatomic simulated spectrum figure 3.5 are by no means similar at first glance. Intensity distribution also looks different. Moreover, simulated spectrum shows much greater number of peaks than the detected spectrum. Nevertheless, by looking closer, especially the line position distribution, the experimental data

and simulated data indeed match each other to some extent. Two sets of well evenly distributed lines could be easily identified in both of the detected and simulated spectrum, as is highlighted in red and green circles. Therefore, these two sets of lines will be used for the identification and comparison thereafter.

First, the agreement between Diatomic simulation and Table of Lyman bands system of H_2 by Abgrall[73] was checked to evaluate the simulation accuracy. The result showed that as long as vibrational quantum number v and rotational quantum number J are smaller than 5, the simulation is quite accurate, with line position discrepancy of less than 1 wavenumber from the tabulated data. However, as v and J increase, the simulated line position starts to deviate from the tabulated position significantly. For higher rotational lines in higher vibrational bands, the deviation could be on the order of hundreds of wavenumbers. Three typical bands are provided here for quantitative comparison in table 3.3 through 3.5.

0-0 band			
line	simulated line position (cm-1)	tabulated line position (cm-1)	difference (cm-1)
P1	90084.26	90085.01	0.75
P2	89887.2	89888.01	0.81
P3	89613.35	89614.17	0.82
P4	89265.08	89266.04	0.96
P5	88845.33	88845.87	0.54
P6	88357.45	88358.73	1.28
P7	87805.07	87805.53	0.46
P8	87191.9	87194	2.1
P9	86521.46	86526.71	5.25
P10	85796.83		
R0	90241.57	90242.36	0.79
R1	90200.38	90201.18	0.8
R2	90079.52	90080.39	0.87
R3	89880.05	89880.94	0.89
R4	89603.72	89604.71	0.99
R5	89252.88	89253.94	1.06
R6	88830.38	88831.83	1.45
R7	88339.49	88341.21	1.72
R8	87783.66	87786.83	3.17

Table 3.3 Line position comparison between Diatomic simulated result and tabulated data for 0-0 band

0-8 band			
line	simulated line position (cm-1)	tabulated line position (cm-1)	difference (cm-1)
P1	63289.25	63300.42	11.17
P2	63184.45	63196.02	11.57
P3	63048.41	63060.75	12.34
P4	62882.86	62896.2	13.34
P5	62689.92	62704.88	14.96
P6	62472.01	62488.68	16.67
P7	62231.75	62250.88	19.13
P8	61971.85	61994.2	22.35
P9	61694.96	61722.52	27.56
P10	61403.47	61438.37	34.9
R0	63400.33	63410.43	10.1
R1	63405.38	63416.56	11.18
R2	63376.77	63388.41	11.64
R3	63315.11	63327.48	12.37
R4	63221.5	63235.35	13.85
R5	63097.47	63112.38	14.91
R6	62944.94	62961.75	16.81
R7	62766.17	62785.35	19.18
R8	62563.61	62586.28	22.67

Table 3.4 Line position comparison between Diatomic simulated result and tabulated data for 0-8 band

6-12 band			
line	simulated line position (cm-1)	tabulated line position (cm-1)	difference (cm-1)
P1	63007.78	63247	239.22
P2	62946.51	63194.43	247.92
P3	62871.48	63133.33	261.85
P4	62784.67	63065.82	281.15
P5	62688.57	62995.32	306.75
P6	62586.12	62925.9	339.78
P7	62480.58	62862.29	381.71
P8	62375.45	62810.77	435.32
P9	62274.29	62778.86	504.57
P10	62180.51	62776.99	596.48
R0	63083.95	63318.48	234.53
R1	63097.83	63336.79	238.96
R2	63095.92	63343.92	248
R3	63079.24	63341.21	261.97
R4	63049.37	63330.63	281.26
R5	63008.43	63315.64	307.21
R6	62959	63299.57	340.57
R7	62904	63286.96	382.96
R8	62846.61	63283.76	437.15

Table 3.5 Line position comparison between Diatomic simulated result and tabulated data for 6-12 band

Since all of the Lyman bands simulation results in the 158-162nm region inevitably suffer from significant deviation from tabulated data, the simulated line position could only be used as a rough reference. A correction of line positions has been tried by first separating all of the rotational lines and adding in a correction coefficient for each rotational line and then adding them up together again. However, this method is extremely tedious and separation of rotational line is by no means straightforward since lots of lines overlap with each other. Another issue here is that the relative intensity is used in Diatomic calculation, which makes the adding up of intensity of different rotational lines and vibrational bands meaningless.

Nevertheless, the earlier pointed out similarity of the line position and intensity distribution between Diatomic simulated data and tabulated data could still be used as a reference to located

and identify those peaks. Obviously, a more accurate line position and intensity reference is needed here for any quantitative analysis for the spectrum. Through a though literature review, the Atlas of the Vacuum Ultraviolet Emission Spectrum of Molecular Hydrogen[105] by Jean-Yves Roncin and Francoise Launay is found to be a very good reference book. The Atlas provides high resolution ultraviolet spectrum of H_2 as well as detailed intensity distribution and line identification.

First of all, the identification of the peaks is performed using the raw simulation data and the result is shown in figure 3.6. As is mentioned above, this identification provides just a rough reference due to the significant uncertainty of line positions.

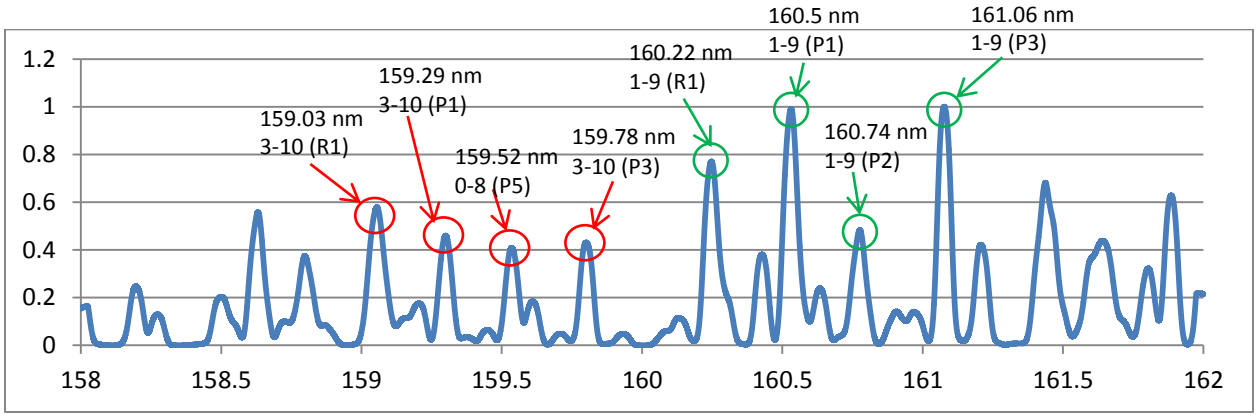

Figure 3.6 spectrum identification of the raw simulation spectrum

Then a more detailed and comprehensive identification is performed using the experimental spectrum, simulated spectrum as well as the Atlas spectrum. The results are shown in table 3.6. The first column indicates the marked order highlighted in figure 3.3. The second column "experimental" presents the detected line position from the above experiment setting. The third column "simulated" comes directly from the Diatomic simulated line positions and descriptions close to the experimentally detected ones. The "tabulated" column represents the line position

and description of peaks almost exactly identical with the experimental data from the H_2 Atlas and the "tabulated intensity" column lists the corresponding intensity. It is obvious that the intensities of some lines are negligible by exactly matching the tabulated line position with the experimental line position, which indicates that the experimental spectrum may not be accurate in terms of line position.

line	experimental (nm)	simulated (nm)	tabulated (nm)	tabulated intensity	Shifted tabulated (nm)	tabulated intensity
R1	158.98	159.03 *3-10(R1)*	159.01 *3-10(R3)*	376	158.88 *3-10(R1)* 158.90 *3-10(R0)* 158.92 *3-10(R2)*	1160 320 250
R2	159.2	159.27 *6-12(P4)* 159.29 *3-10(P1)*	159.21 *6-12(P8)*	18	159.13 *3-10(P1)*	1140
R3	159.43	159.52 *0-8(P5)*	159.45 *7-14(P1)*	63	159.34 *3-10(P2)*	560
R4	159.7	159.78 *3-10(P3)*	159.7 *2-8(R17)*	6	159.61 *3-10(P3)*	1650
Y1	159.98				159.92 *3-10(P4)*	300
G1	160.28	160.22 *1-9(R1)*	160.29 *3-10(P5)*	410	160.2 *1-9(R2)* *4-11 (R1)* 160.21 *4-11(R2)*	 1140 245
G2	160.51	160.5 *3-10(P5)* 160.5 *1-9(P1)*	160.52 *6-13(R1)* *1-9(R4)*	1170	160.43 *1-9(P1)* 160.45 *4-11(P1)*	1215
G3	160.68	160.74 *1-9(P2)*	160.67 *1-9(P2)*	77	160.62 *4-11(P2)*	625
G4	160.9	161.06 *1-9(P3)*	160.9 *6-13 (P3)*	1320	160.84 *4-11(P3)*	1710

Table 3.6 Comprehensive identification of spectrum in the region of 158-162nm

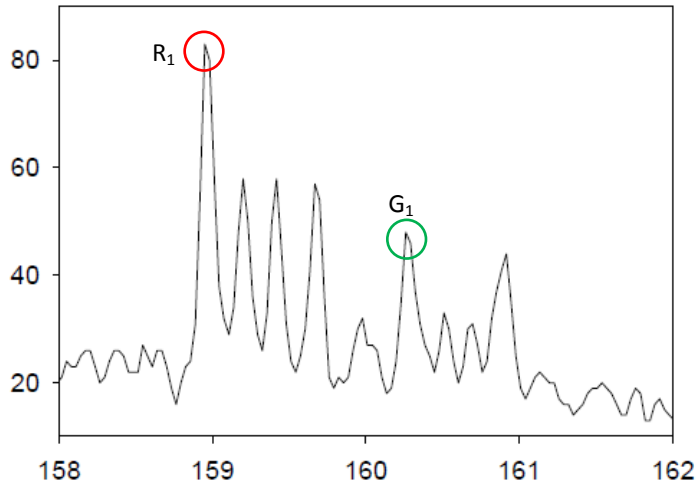

Figure 3.7 magnified experimental spectrum in the region of 158-162nm

Line identification is performed using the H_2 Atlas in the vicinity of each experimental peak. For the R1 line, a flat-top feature is found that at higher resolution the peak is actually a set of closely distributed peaks. By referring to Atlas, a set of closely distributed high intensity lines are easily located, namely the *3-10* band (*R0, R1, R2*) lines. By taking average, the peak should be at 158.90nm. This indicates that the detected line positions are approximately 0.08nm greater than where they are supposed to be. A very similar feature is noticed for the G1 peak and another set of closely distributed high intensity line could be easily found near 160.2nm in the Atlas. Again, they are off by around 0.08nm. These two evidences suggest that the detector scaling may be off by 0.08 nm downwards. By applying this 0.08 nm deviation, the rest of the highly profiled peaks could be perfectly matched with H_2 Atlas as well as their intensities. The shifted data are listed in the "Shifted tabulated" and "tabulated intensity" at the right margin of table 3.6. The averaged deviation is exactly 0.08 nm. The results also suggest that *3-10* band, *1-9* band and *4-11* band are the main contributors to the Lyman band spectrum in the spectrum region of 158nm to 162nm.

4. Conclusion

In this study, detailed literature review is performed with respect to the excimer plasma physics, kinetic and surface physics, vacuum ultraviolet spectrum detection and vacuum handling technique. Also, references concerning Molecular hydrogen Lyman band system is carefully reviewed. An experimental setting custom-designed for the rare-gas excimer VUV system is designed, assembled and tested. Argon and H_2 (3%) mixture is studied using this specific experimental setting. High resolution spectrum is obtained and analyzed. The highly profiled H_2 Lyman bands could serve as a good calibration reference. Meanwhile, a Lyman band simulation is performed using Diatomic code. A comprehensive identification of those detected peaks suggests that our spectrum scaling is off by 0.08nm downward where they are supposed to be. The experimental setting is now ready to be used for more complicated detective purposes in the far ultraviolet region.

References

1. J. Wieser and D. E. Murnick, Vacuum ultraviolet rare gas excimer light source, Rev. Sci. Instrum. 68, 3, 1997.

2. A. Ulrich, J. Wieser, D. E. Murnick, Excimer formation using low energy electron beam excitation, SPIE Vol. 3403 • 0277-786X/98

3. W. Parker, C. Andreen, A simple electron gun for use in electron scattering studies, Nuclear Instruments and Methods, 15, 200-202, 1962.

4. R. Mills, J. He, Y. Lu, M. Nansteel, Z. Chang, B. Dhandapani, Comprehensive identification and potential applications of new states of hydrogen, International Journal of Hydrogen Energy, 32, 2988-3009, 2007.

5. M. W. Cowens, M. M. Blouke, T. Fairchild, J. A. Westphal, Coronene and liumogen as VUV sensitive coatings for Si CCD imagers: a comparison, Applied Optics, Vol. 19, No. 22. 1980.

6. J. A. R. Samson, Techniques of Vacuum Ultraviolet Spectroscopy, Pied Publications, 1967.

7. R. A. Knapp, A simple method for preparing layers of sodium salicylate, Applied Optics, Vol.2, No. 12, December 1963.

8. M. M. Blouke, M. W. Cowens, J. E. Hall, J. A. Westphal, A. B. Christensen, Ultraviolet downconverting phosphor for use with silicon CCD imagers, Applied Optics, Vol. 19, No. 19. 3318-3321. 1980.

9. N. Kristianpoller and D. Dutton, Optical Properties of "Liumogen": A Phosphor for Wavelength Conversion, Applied Optics, Vol. 3, No. 2, 287-290, February 1964.

10. V. Kumar, A. K. Datta, Vacuum ultraviolet scintillators: dosium salicylate and p-terphenyl, Applied Optics, Vol. 18, No.9, 1 May 1979.

11. A. Roth, Vacuum Technology, third, updated and enlarged edition, Elervier Science Publisher B.V. 1990.

12. J. F. O'Hanlan, A User's Guide to Vacuum Technology, third edition, John Wiley & Sons, Inc. 2003.

13. A. Guthrie, Vacuum Technology, John Wiley & Sons, Inc., 1963.

14. A. Chambers, R. K. Fitch and B. S. Halliday, Basic Vacuum Technology, second edition, IOP Publishing Ltd, 1998.

15. Rogers, W.A., Buritz, R.S., Alpert, D. Diffusion Coefficient, Solubility, and Permeability for Helium in Glass, Journal of Applied Physics, Volume: 25 Issue:7, 868 – 875, July 1954.

16. R. L. Mills, J. He, Y. Lu, M. Nansteel, Z. Chang, B. Dhandapani, Comprehensive identification and potential applications of new states of hydrogen, International Journal of Hydrogen Energy, 32, 2988-3009, 2007.

17. M. W. Mallett, Purification of Argon, Industrial and Engineering Chemistry, Vol. 42, No. 10, 2095-2096, October 1950.

18. A. S. Newton, Atomic Energy Commission, MDDC-724, Jan. 1. 1947.

19. G. Bressi, G. Carugno, E. Conti, E. D'Uscio and D. Zanello, Ultra high level argon purification using electron emission from a tip array, Nuclear Instruments and methods in Physics Research, A327, 163-167, 1993.

20. G. Bressi, M. Cambiaghi, G. Carugno, E. Conti, B. Dainese, G. Prete and N. Toniolo, Argon purification in liquid phase, Nuclear Instruments and methods in Physics Research, A 292, 585-592, 1990.

21. P. Cennini, S. Cittolin, L. Dumps, A. Placci, J.P. Revol and C. Rubbia, Argon purification in the liquid phase, Nuclear Instruments and methods in Physics Research, A 333, 567-570, 1993.

22. M. J. Berger and S. M. Seltzer, Tables of energy losses and ranges of electrons and positions, NASA-SP-3012, Jan 01 1964.

23. L. C. Feldman and J. M. Mayer, Fundamentals of surface and thin film analysis, Elsevier Science Publishing Co., Inc. 1986.

24. A. Cohn and G. Caledonia, Spatial Distribution of the Fluorescent Radiation Emission Caused by an Electron Beam, J. Appl. Phys., 41, 3767, 1970.

25. S. Valkealahti, J. Schou and R. M. Nieminen, Energy deposition of keV electrons in light elements, J. Appl. Phys., 65, 2258, 1989.

26. A. Morozov, R. Krücken, A. Ulrich and J. Wieser, Spatial distribution of fluorescent light emitted from neon and nitrogen excited by low energy eletron beams, J. Appl. Phys., 100, 093305, 2006.

27. M. G. Heaps and A. E. S. Green, Energy speading and angular distribution of a beam of electrons in molecular hydrogen, J. Appl. Phys., 46, 4718, 1975.

28. M. G. Heaps and A. E. S. Green, Monte Carlo approach to the spatial deposition of energy by electrons in molecular hydrogen, J. Appl. Phys., 45, 3183, 1974.

29. B. Grosswendt and E. Waibel, Transport of low energy electrons in nitrogen and air, Nuclear Instruments and Methods, 155, 145-156, 1978

30. L. V. Spencer, Theory of Electron Penetration, Physical Review, Vol. 98, No. 6, 1597-1615, June 15th, 1955.

31. M. J. Berger and S. M. Seltzer, Energy deposition by auroral electrons in the atmosphere, Journal of Atmospheric and Terrestrial Physics, Vol. 32, pp. 1015-1045, 1970.

32. A. V. Vasenkov, Nonequilibrium argon plasma generated by an electron beam, Physical Review E, Vol. 57, No. 2, 2212-2221, Feb. 1998.

33. A. E. Z. Grün, Z. Naturforsch. 12a, 89, 1957.

34. B. W. Schumacher, Ontario Research Foundation PRR G401(1964): R. D. Birkhoff, Handbuch Der Physik, edited by S. Flügge(Springer, berlin, 1958), Vol. 34, P. 53.

35. N. F. Mott and H. S. W. Massey, the Theory of Atomic Collisions (Clarendon, Oxford, England), 3rd ed., p. 496. 1965.

36. J. A. R. Samson, Techniques of Vacuum Ultraviolet Spectroscopy, john Wiley & Sons, Inc., 1967.

37. K. Watanabe and F. F. Marmo, Photoionization and Total Absorption Cross Section of Gases. II. O_2 and N_2 in the resion 850-1500 Å, J. Chem. Phys. 25, 965, 1965.

38. P. H. Metzger and G. R. Cook, A Reinvestigation of the Absorption Cross Section of molecular oxygen in the 1050-1800 Å Region, J. Quant. Spectrosc. Radiat. Transfer, Vol. 4, pp. 107-116, 1964.

39. A. C. Allison, A. Dalgarno and N. W. Pasachoff, Absorption by Vibrationally Excited Molecular Oxygen in the Schumann-Runge Continuum, Planet. Space Sci. Vol. 19, pp.1463-1473, 1971.

40. M. Ackerman, F. Biaume and G. Kockarts, Absorption Cross Section of the Schumann-Runge Bands of Molecular Oxygen, Planet. Space Sci. Vol. 18, pp.1639-1651, 1970.

41. K. Yoshino, D. E. Freeman, J. R. Esmond and W. H. Parkinson, High Resolution Absorption Cross Section Measurements and Band Oscillator Strengths of the (1,0)-(12,0) Schumann-Runge Bands of O_2, Planet. Space Sci. Vol. 31, pp. 339-353, 1983.

42. R. W. Ditchburn and P. A. Young, The absorption of molecular oexgen between 1850 and 2500 Å, Journal of Atmospheric and Terrestrial Physics, Vol. 24, pp.127-139, 1962.

43. B. Gellert and U. Kogelschatz, Generation of Excimer Emission in Dielectric Barrier Discharges, Appi. Phys. B 52, 14-21, 1991.

44. A. M. Boichenko, V. S. Skakun, V. F. Tarasenko, E. A. Fomin, and S. I. Yakovienko, Cylindrical Excilanip Pumped by a Barrier Discharge, Laser Physics, Vol. 4, No. 3, pp 635-637, 1994.

45. V. A. Vizir', V. S. Skakun, G. V. Smorudov, E. A. Sosnin, V. F. Tarasenko, E. A. Fomin, V. V. Chervyakov, "Coaxial excimer lamps pumped by barrier and longitudinal discharges, Quantum Electronics 25 (5), 494-497, 1995.

46. A. M. Boichenko, A. N. Panchenko, V. F. Tarasenko, S. I. Yakovlenko, Efficient emission from an He-Xe-NF3 mixture pumped by a glow discharge, Quantum Electronics 26 (5) 407-409, 1996.

47. M. J. Kiik, P. Dube, and B. P. Stoicheff, Spectroscopic study of rare-gas excimer formation in a direct-current discharge with supersonic expansion, J. Chem. Phys. 102 (6), 2351-2364, 1995.

48. T. Efthimiopoulos, D. Zouridis, and A. Ulrich, Excimer emission spectra of rare gas mixtures using either a supersonic expansion or a heavy-ion-beam excitation, J. Phys. D: Appl. Phys. 30, 1 -9, 1997.

49. T. Möller, J. Stapelfeldt, M. Beland and G. Zimmerer, Oscillatory structures in bound-free fluorescence spectra of Xe,Kr2 and Ar2', Chem. Phys. Let., 117 (3), 301-306, 1985.

50. R. H. Lipson, P. E. LaRocque, and B. P. Stoicheff, Vacuum ultraviolet laser spectroscopy. II. Spectra of Xe2 and excited state constants, J. Chem. Phys. 82 (10), 4470-4478, 1985.

51. J. M. Pouvesle, C. Cachoncinile, R. Viladrosa, E. Robert, and A. Khacef, Compact flash X-ray sources and their applications, Nucl. Instr. and Meth. in Phys. Res. B 113, 134-140, 1996.

52. R. Sauerbrey, F. Emmert, and H. Langhoff, Fluorescence and absorption in electron beam excited argOn, J. Phys. B: At. Mol. Phys. 17, 2057-2074, 1984.

53. V. S. Verkhovskii, M. I. Lomaev, A. N. Panchenko, V. F. Tarasenko, 'Foton' series of universal pulsed lasers, Quantum Electronics 25 (1), 5-7, 1995.

54. T. Griegel, H. W. Drotleff, J. W. Hammer, and K. Petkau, The third continuum of the rare gases emitted by heavy ion beam induced plasmas, J. Chem. Phys. 93 (7), 4581-4588, I990.

55. A. Ulrich, H.-J. Körner, W. Krötz, G. Ribitzki, C. E. Murnick, E. Matthias, P. Kienle, and D. H. H. Hoffmann, Heavy-ion excitation of rare-gas excimers, J. Appi. Phys. 62 (2), 357-361, 1987.

56. W. Krötz, A. Ulrich, B. Busch, G. Ribitzki, and J. Wieser, Third excimer continuum of argon excited by a heavy-ion beam, Phys. Rev. A 43 (11), 6089-6094, 1991.

57. B. Busch, A. Ulrich, W. Krötz, G. Ribitzki, J. Wieser, and M. Winkler, Heavy ion beam pumped amplified spontaneous emission on the 172nm xenon excimer transition, J. Appl. Phys. 74 (10), 5960-5963, 1993.

58. G. Ribitzki, A. Ulrich, B. Busch, W. Krötz, J. Wieser, and D. E. Murnick, Electron densities and temperatures in a xenon afterglow with heavy-ion excitation, Phys. Rev. E 50 (5), 3973-3979, 1994.

59. K. P. Huber and G. Herzberg, Molecular Spectra and Molecular Structure IV, Constants of Diatomic Molecules, Litton Educational Publishing, Inc. 1979.

60. T. Lyman, the Spectrum of Hydrogen in the Region of Extremely Short Wave-Lengths, Astrophysical Journal, Vol. 23, p.181, 1906.

61. S. Werner, Hydrogen bands in the ultra-violet Lyman region, Proceedings of the Royal Society of London, Series A, Vol. 113, No. 763, Nov. 1, 1926.

62. H. Abgrall, E. Roueff, F. Launay, J. Roncin and J. Subtil, The lyman and Werner Band Systems of Molecular Hydrogen, Journal of Molecular Spectroscopy, 157, 512-523, 1993.

63. G. H. Dieke and J. J. Hoffield, The Structure of the Ultra-Violet Spectrum of the Hydrogen Molecule, Physical Review, Vol. 30, 400-417, 1927.

64. C. R. Jeppesen, The Emission Spectrum of Molecular Hydrogen in the Extreme Ultraviolet, Phys. Rev. 44, 165-184, 1933.

65. A. Monfils, The absorption spectra if the molecules H_2, HD and D_2 Part VI., Journal of Molecular Spectroscopy, Volume 15, Issue 3, Pages 265-307, 1965.

66. T. Namioka, Absorption Spectra of H_2 in the Vacuum Ultraviolet Region. II. The B'-X, B"-X, D-X and D'-X Bands, J. Chem. Phys. 41, 2141, 1964.

67. Sanzo Takezawa, Absorption Spectrum of H_2 in the vacuum –uv Region. I. Rydberg States and Ionization Energies, J. Chem. Phys. 52, 2575, 1970.

68. G. Herzberg and Ch. Jungen, Gydberg series and ionization potential of the H_2 molecule, Journal of Molecular Spectroscopy, Volume 41, Issue 3, Pages 425-486, 1972.

69. G. Herzberg and L. L. Howe, the Lyman Bands of Molecular Hydrogen, Can. J. Phys. Vol. 37, 636, 1959.

70. I. Dabrowski, The Lyman and Werner Bands of H_2, Can. J. Phys. Vol. 62, 1639, 1984.

71. J. Roncin, F. Launay and M. Larzilliere, High resolution emission spectrum of H_2 between 78 and 118 nm, Can. J. Phys. 62(12): 1686-1705, 1984.

72. M. Larzilliere, F. Launay and J. Roncin, Refined molecular constants for the $C^1\prod_u^+$ states of H_2, Can. J. Phys. 63(11): 1416-1417, 1985.

73. H. Abgrall, E. Roueff, F. Launay, J. Roncin and J. Subtil, Table of the Lyman band system of molecular hydrogen, Astron. Astrophys. Suppl. Ser. 101, p.273-321, 1993.

74. H. Abgrall, E. Roueff, F. Launay, J. Roncin and J. Subtil, The Lyman and Werner band systems of molecular hydrogen J. Mol. Spectrosc. 157, p.512-523, 1993.

75. M. A. Baig and J. P. Connerade, New high-resolution photoabsorption study of the Lyman bands of H2, J. Phys. B: At. Mol. Phys. 18, p.809-813, 1985.

76. Ch. Jungen, I. Dabrowski, G. Herzberg and M. Vervloet High orbital angular momentum states in H2 and D2: III. Singlet-triplet splittings, energy levels, and ionization potentials, J. Chem. Phys. 93, p.2289-98, 1990.

77. P. C. Hinnen, W. Hogervorst, S. Stolte and W. Ubachs, Sub-Doppler laser spectroscopy of H2 and D2 in the range 91-98 nm, Can. J. Phys. 72, p.1032-1042, 1994.

78. W. Reinhold, W. Hogervorst and W. Ubachs, High resolution laser spectroscopy of H2 at 86–90 nm, J. Mol. Spectrosc. 180, p.156-163, 1996.

79. U. Hollenstein, E. Reinhold C. A. de Lange and W. Ubachs, High-resolution VUV-laser spectroscopic study of the $B^1\Sigma^+_u$ (v' = 0-2)← $X^1\Sigma^+_g$ (v" = 0) Lyman bands in H_2 and HD, J. Phys. B: At. Mol. Opt. Phys. 39, L195-L201, 2006

80. J. Philip, J. P. Sprengers, Th. Pielage, C. A. de Lange, W. Ubachs and E. Reinhold, Highly accurate transition frequencies in the H2 Lyman and Werner absorption bands, Can. J. Chem. 82, p.713-22, 2004.

81. J.T. Vanderslice, E.A. Mason and W.G. Maisch, Ground state of hydrogen by the Rydberg-Kelein-Rees method, Volume 3, Issues 1–6, Pages 17–29, 1959.

82. I. Tobias and J. T. Vanderslice, Potential Energy Curves for the $X^1\Sigma^+_g$ and $B^1\Sigma^+_u$ States of Hydrogen, J. Chems. Phys. 35, 1852, 1961.

83. R. W. Nicholls, Franck-Condon Factors for the H_2 Lyman-Band System, Astrophysical Journal , vol. 141, p.819, 1965.

84. W. R. Jarmain and R. W. Nicholls, A theoretical study of the O_2 $X^3\Sigma^-_g$ - $B^3\Sigma^-_u$ photodissociation continuum, Proc. Phys. Soc. 84, 417, 1964.

85. P. S. Julienne, Nonadiabatic effects in the B, C, B' and D states of H_2, Journal of Molecular Spectroscopy, Volume 48, Issue 3, Pages 508-529, 1973.

86. A. L. Ford, K. K. Docken and A. Dalgarno, The Photoionization and Dissociative Photoionization of H_2, HD and D_2, Astophysical Journal, Vol. 195, pt. 1, p. 819-824, 1975.

87. H. Abgrall, F. Launay, E. Roueff and J. Roncin, Effect of rotational coupling on emission probabilities of Lyman and Werner band systems of the vacuum ultraviolet spectrum of H_2, Journal of Chemical Physics, Volume 87, Issue 4, p. 2036, 1987.

88. H. Abgrall and E. Roueff, Wavelengths, oscillator strengths and transition probabilities of H_2 molecule for Lyman and Werner systems, Astron. Astrophys. Suppl. Ser., 79, 313-328, 1989.

89. P. Senn, P. Quadrelli and K. Dressler, The $B\,^1\Sigma^+_u$, $B'\,^1\Sigma^+_u$, $C\,^1\Pi_u$, and $D\,^1\Pi_u$ states of hydrogen. *Ab initio* calculation of rovibronic coupling in H_2, HD, and D_2, J. Chem. Phys., 89, 7401, 1988.

90. R. Mohan Sankaran, Konstantinos, P. Giapis, Mohamed Moselhy and Karl H. Schoenbach, Argon excimer emission from high-pressure microdischarges in metal capillaries, Appl. Phys. Lett., 83, 4728, 2003.

91. M.Moselhy, I. Petzenhauser, K. Frank and K. H. Schoenbach, Excimer emission from microhollow cathode argon discharges, J. Phys. D: Appl. Phys., 36, 2922, 2003.

92. Karl H. Schoenbach, Ahmed El-Habachi, Mohamed M. Moselhy, Wenhui Shi, and Robert H. Stark, Microhollow cathode discharge excimer lamps, Phys. Plasmas, 7, 2186, 2000.

93. S. Kucodera, M. Honda, M. Kitahara, J. Kawanaka, W. Sasaki and K. Kurosawa, Extended Broad-band Emission in Vacuum Ultraviolet by Multi-Rare-Gas Silent Discharges, Jpn. J. Appl. Phys., Vol. 34, pp. L618-L620, 1995.

94. N. Masoud, K. Martus and K. Becker, VUV emission from a cylindrical dielectric barrier discharge in Ar and in Ar/N2 and Ar/air mixtures, J. Phys. D: Appl. Phys., 38, 1674, 2005.

95. S. Kubodera, M. Kitahara, J. Kawanaka, W. Sasaki, and K. Kurosawa, A vacuum ultraviolet flash lamp with extremely broadened emission spectra, Appl. Phys. Lett., 69, 452, 1996.

96. B. Eliasson and U. Kogelschatz, UV Excimer Radiation from Dielectric-Barrier Discharges, Appl. Phys. B, 46, 299-303, 1988.

97. A. El-Habachi and K. H. Schoenbach, Emission of excimer radiation from direct current, high-pressure hollow cathode discharges, Appl. Phys. Lett., 72, 22, 1998.

98. A. El-Habachi and K. H. Schoenbach, Generation of intense excimer radiation from high-pressure hollow cathode Discharges, Appl. Phys. Lett., 73, 885, 1998.

99. W.-G. Lee, M. Shao, J. R. Gottschalk, M. Brown, and A. D. Compaan, Vacuum ultraviolet emission dynamics of a coplanar electrode microdischarge: dependence on voltage and Xe concentration, J. Appl. Phys., 92, 682, 2002.

100. S. Liu and M. Neiger, Double discharges in unipolar-pulsed dielectric barrier discharge xenon excimer lamps, J. Phys. D: Appl. Phys., 36, 1565, 2003.

101. R. J. Carman and R. P. Mildren, Computer modelling of a short-pulse excited dielectric barrier discharge xenon excimer lamp(λ~172 nm), J. Phys. D: Appl. Phys., 36, 19, 2003.

102. P Kurunczi, H Shah and K Becker, Hydrogen Lyman-α and Lyman-β emissions from high-pressure microhollow cathode discharges in Ne–H2 mixtures, J. Phys. B: At. Mol. Opt. Phys., 32, 1999.

103. F. Mühlberger, J. Wieser, A. Morozov, A. Ulrich, and R. Zimmermann, Single-Photon Ionization Quadrupole Mass Spectrometry with an Electron Beam Pumped Excimer Light Source, Anal. Chem., 77, 2218-2226, 2005.

104. T. Oppenländer, S. Gliese, Mineralization of organic micropollutants (homologous alcohols and phenols) in water by vacuum-UV-oxidation (H2O-VUV) with an incoherent xenon-excimer lamp at 172 nm, Chemosphere, 40, 15-21, 2000.

105. J. Roncin and F. Launay, Atlas of the Vacuum Ultraviolet Emission Spectrum of Molecular Hydrogen, National Institute of Standards and Technology, 1994.

Appendix

Complete simulated data of Lyman band molecular hydrogen using Diatomic program.

Brh.	j',p'	-	j",p"	Erot_u(cm-1)	Erot_l(cm-1)	LinePosition(cm-1)	LineStrength	RotPopulation	Intensity
0-8 band									
P	0,e	-	1,e	0	72.24447	63289.25	1	0.133805	0.1987
P	1,e	-	2,e	38.8316	215.8789	63184.45	2	0.111069	0.109958
P	2,e	-	3,e	116.1242	429.2169	63048.41	3	0.383329	0.341546
P	3,e	-	4,e	231.1469	709.7873	62882.86	4	0.103039	0.087436
P	4,e	-	5,e	382.8284	1054.406	62689.92	5	0.192015	0.158413
P	5,e	-	6,e	569.7876	1459.277	62472.01	6	0.031912	0.025849
P	6,e	-	7,e	790.374	1920.126	62231.75	7	0.03928	0.031409
P	7,e	-	8,e	1042.718	2432.371	61971.85	8	0.004504	0.003567
P	8,e	-	9,e	1324.793	2991.335	61694.96	9	0.003959	0.003112
P	9,e	-	10,e	1634.484	3592.509	61403.47	10	0.000334	0.000261
R	1,e	-	0,e	38.8316	0	63400.33	1	0.111069	0.054979
R	2,e	-	1,e	116.1242	72.24447	63405.38	2	0.383329	0.227697
R	3,e	-	2,e	231.1469	215.8789	63376.77	3	0.103039	0.065577
R	4,e	-	3,e	382.8284	429.2169	63315.11	4	0.192015	0.12673
R	5,e	-	4,e	569.7876	709.7873	63221.5	5	0.031912	0.021541
R	6,e	-	5,e	790.374	1054.406	63097.47	6	0.03928	0.026922
R	7,e	-	6,e	1042.718	1459.277	62944.94	7	0.004504	0.003121
R	8,e	-	7,e	1324.793	1920.126	62766.17	8	0.003959	0.002766
R	9,e	-	8,e	1634.484	2432.371	62563.61	9	0.000334	0.000235
1-9 band									
P	0,e	-	1,e	0	66.10028	62304.86	1	0.127565	0.463978
P	1,e	-	2,e	36.91467	197.4599	62210.42	2	0.106867	0.25913
P	2,e	-	3,e	110.4168	392.4185	62088.96	3	0.375593	0.819665
P	3,e	-	4,e	219.8605	648.5405	61942.28	4	0.103698	0.215525
P	4,e	-	5,e	364.2992	962.6834	61772.58	5	0.200073	0.404281
P	5,e	-	6,e	542.5113	1331.093	61582.38	6	0.034676	0.068794
P	6,e	-	7,e	753.0355	1749.531	61374.47	7	0.044793	0.087726
P	7,e	-	8,e	994.2146	2213.432	61151.75	8	0.005419	0.010511
P	8,e	-	9,e	1264.248	2718.109	60917.1	9	0.005046	0.009716
P	9,e	-	10,e	1561.252	3259.001	60673.21	10	0.000452	0.000866
R	1,e	-	0,e	36.91467	0	62407.88	1	0.106867	0.129565

R	2,e	-	1,e	110.4168	66.10028	62415.28	2	0.375593	0.546443
R	3,e	-	2,e	219.8605	197.4599	62393.36	3	0.103698	0.161644
R	4,e	-	3,e	364.2992	392.4185	62342.84	4	0.200073	0.323425
R	5,e	-	4,e	542.5113	648.5405	62264.93	5	0.034676	0.057329
R	6,e	-	5,e	753.0355	962.6834	62161.32	6	0.044793	0.075194
R	7,e	-	6,e	994.2146	1331.093	62034.08	7	0.005419	0.009197
R	8,e	-	7,e	1264.248	1749.531	61885.68	8	0.005046	0.008636
R	9,e	-	8,e	1561.252	2213.432	61718.78	9	0.000452	0.000779
2-9 band									
P	0,e	-	1,e	0	66.10028	63586.37	1	0.122166	0.184715
P	1,e	-	2,e	35.25189	197.4599	63490.27	2	0.103163	0.103989
P	2,e	-	3,e	105.4655	392.4185	63365.52	3	0.368341	0.33416
P	3,e	-	4,e	210.0679	648.5405	63214	4	0.104084	0.089929
P	4,e	-	5,e	348.218	962.6834	63038.01	5	0.206968	0.173854
P	5,e	-	6,e	518.829	1331.093	62840.21	6	0.037203	0.030682
P	6,e	-	7,e	720.5976	1749.531	62623.54	7	0.050117	0.040803
P	7,e	-	8,e	952.0411	2213.432	62391.08	8	0.006353	0.005123
P	8,e	-	9,e	1211.542	2718.109	62145.91	9	0.006222	0.004981
P	9,e	-	10,e	1497.398	3259.001	61890.87	10	0.000588	0.000468
R	1,e	-	0,e	35.25189	0	63687.73	1	0.103163	0.051994
R	2,e	-	1,e	105.4655	66.10028	63691.84	2	0.368341	0.222773
R	3,e	-	2,e	210.0679	197.4599	63665.08	3	0.104084	0.067447
R	4,e	-	3,e	348.218	392.4185	63608.27	4	0.206968	0.139083
R	5,e	-	4,e	518.829	648.5405	63522.76	5	0.037203	0.025568
R	6,e	-	5,e	720.5976	962.6834	63410.39	6	0.050117	0.034974
R	7,e	-	6,e	952.0411	1331.093	63273.42	7	0.006353	0.004482
R	8,e	-	7,e	1211.542	1749.531	63114.49	8	0.006222	0.004427
R	9,e	-	8,e	1497.398	2213.432	62936.44	9	0.000588	0.000421
2-10 band									
P	0,e	-	1,e	0	59.72312	61533.66	1	0.122166	0.62062
P	1,e	-	2,e	35.25189	178.3386	61450.29	2	0.103163	0.349389
P	2,e	-	3,e	105.4655	354.2055	61344.64	3	0.368341	1.122735
P	3,e	-	4,e	210.0679	584.9136	61218.53	4	0.104084	0.30215
P	4,e	-	5,e	348.218	867.3489	61074.25	5	0.206968	0.584126
P	5,e	-	6,e	518.829	1197.782	60914.43	6	0.037203	0.103088
P	6,e	-	7,e	720.5976	1571.989	60741.99	7	0.050117	0.137094
P	7,e	-	8,e	952.0411	1985.4	60560.02	8	0.006353	0.017212

P	8,e	-	9,e	1211.542	2433.291	60371.63	9	0.006222	0.016734
P	9,e	-	10,e	1497.398	2911.018	60179.76	10	0.000588	0.001573
R	1,e	-	0,e	35.25189	0	61628.63	1	0.103163	0.174695
R	2,e	-	1,e	105.4655	59.72312	61639.12	2	0.368341	0.74849
R	3,e	-	2,e	210.0679	178.3386	61625.11	3	0.104084	0.226612
R	4,e	-	3,e	348.218	354.2055	61587.39	4	0.206968	0.4673
R	5,e	-	4,e	518.829	584.9136	61527.3	5	0.037203	0.085906
R	6,e	-	5,e	720.5976	867.3489	61446.63	6	0.050117	0.117509
R	7,e	-	6,e	952.0411	1197.782	61347.64	7	0.006353	0.01506
R	8,e	-	7,e	1211.542	1571.989	61232.93	8	0.006222	0.014875
R	9,e	-	8,e	1497.398	1985.4	61105.38	9	0.000588	0.001416
3-10 band									
P	0,e	-	1,e	0	59.72312	62780.15	1	0.117427	0.183183
P	1,e	-	2,e	33.79048	178.3386	62695.33	2	0.099859	0.103852
P	2,e	-	3,e	101.1121	354.2055	62586.78	3	0.361522	0.338379
P	3,e	-	4,e	201.4522	584.9136	62456.41	4	0.104267	0.092945
P	4,e	-	5,e	334.0568	867.3489	62306.58	5	0.21292	0.184527
P	5,e	-	6,e	497.9487	1197.782	62140.04	6	0.039526	0.033632
P	6,e	-	7,e	691.9514	1571.989	61959.84	7	0.055268	0.046424
P	7,e	-	8,e	914.7194	1985.4	61769.19	8	0.007303	0.006076
P	8,e	-	9,e	1164.774	2433.291	61571.36	9	0.007484	0.006181
P	9,e	-	10,e	1440.545	2911.018	61369.4	10	0.000743	0.00061
R	1,e	-	0,e	33.79048	0	62873.66	1	0.099859	0.051926
R	2,e	-	1,e	101.1121	59.72312	62881.26	2	0.361522	0.225586
R	3,e	-	2,e	201.4522	178.3386	62862.99	3	0.104267	0.069709
R	4,e	-	3,e	334.0568	354.2055	62819.73	4	0.21292	0.147622
R	5,e	-	4,e	497.9487	584.9136	62752.91	5	0.039526	0.028027
R	6,e	-	5,e	691.9514	867.3489	62664.48	6	0.055268	0.039792
R	7,e	-	6,e	914.7194	1197.782	62556.81	7	0.007303	0.005317
R	8,e	-	7,e	1164.774	1571.989	62432.66	8	0.007484	0.005494
R	9,e	-	8,e	1440.545	1985.4	62295.02	9	0.000743	0.000549
4-11 band									
P	0,e	-	1,e	0	53.06741	62200.6	1	0.112502	0.171837
P	1,e	-	2,e	32.47762	158.3784	62127.76	2	0.096275	0.098034
P	2,e	-	3,e	97.19812	314.3043	62036.56	3	0.352923	0.323435
P	3,e	-	4,e	193.6967	518.4508	61928.91	4	0.10368	0.090492
P	4,e	-	5,e	321.2876	767.7183	61807.23	5	0.216873	0.18403

P	5,e	-	6,e	479.0784	1058.386	61674.36	6	0.041455	0.034538
P	6,e	-	7,e	665.9882	1386.224	61533.43	7	0.059971	0.049323
P	7,e	-	8,e	880.7712	1746.635	61387.8	8	0.008234	0.006708
P	8,e	-	9,e	1122.044	2134.83	61240.88	9	0.008801	0.007117
P	9,e	-	10,e	1388.319	2546.051	61095.93	10	0.000914	0.000735
R	1,e	-	0,e	32.47762	0	62286.14	1	0.096275	0.049017
R	2,e	-	1,e	97.19812	53.06741	62297.79	2	0.352923	0.215623
R	3,e	-	2,e	193.6967	158.3784	62288.98	3	0.10368	0.067869
R	4,e	-	3,e	321.2876	314.3043	62260.65	4	0.216873	0.147224
R	5,e	-	4,e	479.0784	518.4508	62214.29	5	0.041455	0.028781
R	6,e	-	5,e	665.9882	767.7183	62151.93	6	0.059971	0.042277
R	7,e	-	6,e	880.7712	1058.386	62076.05	7	0.008234	0.005869
R	8,e	-	7,e	1122.044	1386.224	61989.48	8	0.008801	0.006326
R	9,e	-	8,e	1388.319	1746.635	61895.35	9	0.000914	0.000662
5-11 band									
P	0,e	-	1,e	0	53.06741	63380.3	1	0.108452	0.054138
P	1,e	-	2,e	31.26053	158.3784	63306.25	2	0.093353	0.031067
P	2,e	-	3,e	93.56519	314.3043	63212.62	3	0.346199	0.103691
P	3,e	-	4,e	186.4845	518.4508	63101.4	4	0.103465	0.029513
P	4,e	-	5,e	309.3824	767.7183	62975.03	5	0.221351	0.061386
P	5,e	-	6,e	461.4261	1058.386	62836.4	6	0.043493	0.011843
P	6,e	-	7,e	641.5992	1386.224	62688.74	7	0.064986	0.017468
P	7,e	-	8,e	848.718	1746.635	62535.45	8	0.009257	0.002464
P	8,e	-	9,e	1081.451	2134.83	62379.99	9	0.010308	0.002724
P	9,e	-	10,e	1338.343	2546.051	62225.66	10	0.00112	0.000294
R	1,e	-	0,e	31.26053	0	63464.62	1	0.093353	0.015534
R	2,e	-	1,e	93.56519	53.06741	63473.86	2	0.346199	0.069127
R	3,e	-	2,e	186.4845	158.3784	63461.47	3	0.103465	0.022135
R	4,e	-	3,e	309.3824	314.3043	63428.44	4	0.221351	0.049109
R	5,e	-	4,e	461.4261	518.4508	63376.34	5	0.043493	0.009869
R	6,e	-	5,e	641.5992	767.7183	63307.24	6	0.064986	0.014972
R	7,e	-	6,e	848.718	1058.386	63223.7	7	0.009257	0.002156
R	8,e	-	7,e	1081.451	1386.224	63128.59	8	0.010308	0.002421
R	9,e	-	8,e	1338.343	1746.635	63025.07	9	0.00112	0.000265
5-12 band									
P	0,e	-	1,e	0	46.08754	61860.86	1	0.108452	0.157376
P	1,e	-	2,e	31.26053	137.4423	61800.77	2	0.093353	0.09031

P	2,e	-	3,e	93.56519	272.4414	61728.07	3	0.346199	0.301423
P	3,e	-	4,e	186.4845	448.696	61644.74	4	0.103465	0.085794
P	4,e	-	5,e	309.3824	663.1078	61553.22	5	0.221351	0.178447
P	5,e	-	6,e	461.4261	911.9477	61456.43	6	0.043493	0.034426
P	6,e	-	7,e	641.5992	1190.96	61357.59	7	0.064986	0.050778
P	7,e	-	8,e	848.718	1495.494	61260.17	8	0.009257	0.007164
P	8,e	-	9,e	1081.451	1820.672	61167.73	9	0.010308	0.007919
P	9,e	-	10,e	1338.343	2161.592	61083.7	10	0.00112	0.000856
R	1,e	-	0,e	31.26053	0	61938.21	1	0.093353	0.045155
R	2,e	-	1,e	93.56519	46.08754	61954.43	2	0.346199	0.200949
R	3,e	-	2,e	186.4845	137.4423	61955.99	3	0.103465	0.064345
R	4,e	-	3,e	309.3824	272.4414	61943.89	4	0.221351	0.142757
R	5,e	-	4,e	461.4261	448.696	61919.68	5	0.043493	0.028688
R	6,e	-	5,e	641.5992	663.1078	61885.44	6	0.064986	0.043524
R	7,e	-	6,e	848.718	911.9477	61843.72	7	0.009257	0.006268
R	8,e	-	7,e	1081.451	1190.96	61797.44	8	0.010308	0.007039
R	9,e	-	8,e	1338.343	1495.494	61749.8	9	0.00112	0.00077
6-12 band									
P	0,e	-	1,e	0	46.08754	63007.78	1	0.104512	0.064635
P	1,e	-	2,e	30.08639	137.4423	62946.51	2	0.090469	0.0373
P	2,e	-	3,e	90.0549	272.4414	62871.48	3	0.339285	0.125897
P	3,e	-	4,e	179.4989	448.696	62784.67	4	0.103103	0.036436
P	4,e	-	5,e	297.8132	663.1078	62688.57	5	0.225479	0.07747
P	5,e	-	6,e	444.1998	911.9477	62586.12	6	0.045523	0.015356
P	6,e	-	7,e	617.6755	1190.96	62480.58	7	0.070239	0.02339
P	7,e	-	8,e	817.0815	1495.494	62375.45	8	0.010382	0.003424
P	8,e	-	9,e	1041.095	1820.672	62274.29	9	0.012055	0.003947
P	9,e	-	10,e	1288.241	2161.592	62180.51	10	0.001373	0.000447
R	1,e	-	0,e	30.08639	0	63083.95	1	0.090469	0.01865
R	2,e	-	1,e	90.0549	46.08754	63097.83	2	0.339285	0.083932
R	3,e	-	2,e	179.4989	137.4423	63095.92	3	0.103103	0.027327
R	4,e	-	3,e	297.8132	272.4414	63079.24	4	0.225479	0.061976
R	5,e	-	4,e	444.1998	448.696	63049.37	5	0.045523	0.012797
R	6,e	-	5,e	617.6755	663.1078	63008.43	6	0.070239	0.020049
R	7,e	-	6,e	817.0815	911.9477	62959	7	0.010382	0.002996
R	8,e	-	7,e	1041.095	1190.96	62904	8	0.012055	0.003508
R	9,e	-	8,e	1288.241	1495.494	62846.61	9	0.001373	0.000402
6-13 band									

P	0,e	-	1,e	0	38.7379	61775.51	1	0.104512	0.126815
P	1,e	-	2,e	30.08639	115.3935	61728.94	2	0.090469	0.073183
P	2,e	-	3,e	90.0549	228.3431	61675.96	3	0.339285	0.247012
P	3,e	-	4,e	179.4989	375.1932	61618.55	4	0.103103	0.071489
P	4,e	-	5,e	297.8132	552.8333	61559.23	5	0.225479	0.151997
P	5,e	-	6,e	444.1998	757.509	61500.94	6	0.045523	0.03013
P	6,e	-	7,e	617.6755	984.9186	61447.01	7	0.070239	0.045892
P	7,e	-	8,e	817.0815	1230.336	61400.99	8	0.010382	0.006718
P	8,e	-	9,e	1041.095	1488.766	61366.58	9	0.012055	0.007744
P	9,e	-	10,e	1288.241	1755.133	61347.36	10	0.001373	0.000877
R	1,e	-	0,e	30.08639	0	61844.34	1	0.090469	0.036592
R	2,e	-	1,e	90.0549	38.7379	61865.57	2	0.339285	0.164675
R	3,e	-	2,e	179.4989	115.3935	61878.35	3	0.103103	0.053616
R	4,e	-	3,e	297.8132	228.3431	61883.72	4	0.225479	0.121598
R	5,e	-	4,e	444.1998	375.1932	61883.26	5	0.045523	0.025108
R	6,e	-	5,e	617.6755	552.8333	61879.09	6	0.070239	0.039336
R	7,e	-	6,e	817.0815	757.509	61873.82	7	0.010382	0.005879
R	8,e	-	7,e	1041.095	984.9186	61870.42	8	0.012055	0.006883
R	9,e	-	8,e	1288.241	1230.336	61872.15	9	0.001373	0.000789
7-13 band									
P	0,e	-	1,e	0	38.7379	62889.38	1	0.100498	0.092724
P	1,e	-	2,e	28.90242	115.3935	62841.62	2	0.08749	0.053815
P	2,e	-	3,e	86.50885	228.3431	62786.28	3	0.33185	0.183709
P	3,e	-	4,e	172.4231	375.1932	62725.34	4	0.102566	0.054075
P	4,e	-	5,e	286.052	552.8333	62661.33	5	0.2294	0.117587
P	5,e	-	6,e	426.6075	757.509	62597.21	6	0.047628	0.02397
P	6,e	-	7,e	593.1084	984.9186	62536.3	7	0.075987	0.037751
P	7,e	-	8,e	784.3832	1230.336	62482.16	8	0.011678	0.005746
P	8,e	-	9,e	999.0733	1488.766	62438.42	9	0.01418	0.006926
P	9,e	-	10,e	1235.637	1755.133	62408.62	10	0.001699	0.000825
R	1,e	-	0,e	28.90242	0	62957.02	1	0.08749	0.026908
R	2,e	-	1,e	86.50885	38.7379	62975.89	2	0.33185	0.122473
R	3,e	-	2,e	172.4231	115.3935	62985.14	3	0.102566	0.040557
R	4,e	-	3,e	286.052	228.3431	62985.82	4	0.2294	0.094069
R	5,e	-	4,e	426.6075	375.1932	62979.53	5	0.047628	0.019975
R	6,e	-	5,e	593.1084	552.8333	62968.39	6	0.075987	0.032358
R	7,e	-	6,e	784.3832	757.509	62954.99	7	0.011678	0.005028
R	8,e	-	7,e	999.0733	984.9186	62942.27	8	0.01418	0.006157

R	9,e	-	8,e	1235.637	1230.336	62933.42	9	0.001699	0.000742
7-14 band									
P	0,e	-	1,e	0	30.97291	61960.53	1	0.100498	0.035415
P	1,e	-	2,e	28.90242	92.09533	61928.31	2	0.08749	0.020554
P	2,e	-	3,e	86.50885	181.7358	61896.27	3	0.33185	0.070166
P	3,e	-	4,e	172.4231	297.4863	61866.44	4	0.102566	0.020654
P	4,e	-	5,e	286.052	436.2107	61841.34	5	0.2294	0.044911
P	5,e	-	6,e	426.6075	594.1125	61823.99	6	0.047628	0.009155
P	6,e	-	7,e	593.1084	766.8239	61817.78	7	0.075987	0.014419
P	7,e	-	8,e	784.3832	949.5201	61826.36	8	0.011678	0.002195
P	8,e	-	9,e	999.0733	1137.061	61853.51	9	0.01418	0.002645
P	9,e	-	10,e	1235.637	1324.166	61902.97	10	0.001699	0.000315
R	1,e	-	0,e	28.90242	0	62020.4	1	0.08749	0.010277
R	2,e	-	1,e	86.50885	30.97291	62047.04	2	0.33185	0.046777
R	3,e	-	2,e	172.4231	92.09533	62071.83	3	0.102566	0.01549
R	4,e	-	3,e	286.052	181.7358	62095.82	4	0.2294	0.035929
R	5,e	-	4,e	426.6075	297.4863	62120.62	5	0.047628	0.007629
R	6,e	-	5,e	593.1084	436.2107	62148.4	6	0.075987	0.012359
R	7,e	-	6,e	784.3832	594.1125	62181.77	7	0.011678	0.00192
R	8,e	-	7,e	999.0733	766.8239	62223.75	8	0.01418	0.002352
R	9,e	-	8,e	1235.637	949.5201	62277.62	9	0.001699	0.000284